CANADIAN THESES ON MICROFICHE

I.S.B.N.

THESES CANADIENNES SUR MICROFICHE

National Library of Canada
Collections Development Branch

Canadian Theses on
Microfiche Service

Ottawa, Canada
K1A 0N4

Bibliothèque nationale du Canada
Direction du développement des collections

Service des thèses canadiennes
sur microfiche

NOTICE

The quality of this microfiche is heavily dependent upon the quality of the original thesis submitted for microfilming. Every effort has been made to ensure the highest quality of reproduction possible.

If pages are missing, contact the university which granted the degree.

Some pages may have indistinct print especially if the original pages were typed with a poor typewriter ribbon or if the university sent us a poor photocopy.

Previously copyrighted materials (journal articles, published tests, etc.) are not filmed.

Reproduction in full or in part of this film is governed by the Canadian Copyright Act, R.S.C. 1970, c. C-30. Please read the authorization forms which accompany this thesis.

AVIS

La qualité de cette microfiche dépend grandement de la qualité de la thèse soumise au microfilmage. Nous avons tout fait pour assurer une qualité supérieure de reproduction.

S'il manque des pages, veuillez communiquer avec l'université qui a conféré le grade.

La qualité d'impression de certaines pages peut laisser à désirer, surtout si les pages originales ont été dactylographiées à l'aide d'un ruban usé ou si l'université nous a fait parvenir une photocopie de mauvaise qualité.

Les documents qui font déjà l'objet d'un droit d'auteur (articles de revue, examens publiés, etc.) ne sont pas microfilmés.

La reproduction, même partielle, de ce microfilm est soumise à la Loi canadienne sur le droit d'auteur, SRC 1970, c. C-30. Veuillez prendre connaissance des formules d'autorisation qui accompagnent cette thèse.

THIS DISSERTATION
HAS BEEN MICROFILMED
EXACTLY AS RECEIVED

LA THÈSE A ÉTÉ
MICROFILMÉE TELLE QUE
NOUS L'AVONS REÇUE

NL-339 (r. 82/08)

Canada

70.

0-315-15979-0

National Library of Canada | Bibliothèque nationale du Canada

Canadian Theses Division | Division des thèses canadiennes

Ottawa, Canada
K1A 0N4

63888

PERMISSION TO MICROFILM — AUTORISATION DE MICROFILMER

• Please print or type — Écrire en lettres moulées ou dactylographier

Full Name of Author — Nom complet de l'auteur

CALVIN WAYNE DOMIER

Date of Birth — Date de naissance	Country of Birth — Lieu de naissance
APRIL 7, 1958	CANADA

Permanent Address — Résidence fixe

11759 - 37 Avenue
Edmonton, Alberta
Canada

Title of Thesis — Titre de la thèse

Image Analysis as a Diagnostic Aid in Laser Research

University — Université

University of Alberta

Degree for which thesis was presented — Grade pour lequel cette thèse fut présentée

Master of Science

Year this degree conferred — Année d'obtention de ce grade	Name of Supervisor — Nom du directeur de thèse
1983	Dr. A.A. Offenberger

Permission is hereby granted to the NATIONAL LIBRARY OF CANADA to microfilm this thesis and to lend or sell copies of the film.

The author reserves other publication rights, and neither the thesis nor extensive extracts from it may be printed or otherwise reproduced without the author's written permission.

L'autorisation est, par la présente, accordée à la BIBLIOTHÈQUE NATIONALE DU CANADA de microfilmer cette thèse et de prêter ou de vendre des exemplaires du film.

L'auteur se réserve les autres droits de publication; ni la thèse ni de longs extraits de celle-ci ne doivent être imprimés ou autrement reproduits sans l'autorisation écrite de l'auteur.

Date	Signature
March 31, 1983	Calvin Wayne Domier

NL-91 (4/77)

THE UNIVERSITY OF ALBERTA

Image Analysis as a Diagnostic Aid in Laser Research

by

Calvin Wayne Domier

A THESIS

SUBMITTED TO THE FACULTY OF GRADUATE STUDIES AND RESEARCH

IN PARTIAL FULFILMENT OF THE REQUIREMENTS FOR THE DEGREE

OF Master of Science

Department of Electrical Engineering

EDMONTON, ALBERTA

Spring, 1983

THE UNIVERSITY OF ALBERTA

RELEASE FORM

NAME OF AUTHOR Calvin Wayne Domier

TITLE OF THESIS Image Analysis as a Diagnostic Aid in Laser Research

DEGREE FOR WHICH THESIS WAS PRESENTED Master of Science

YEAR THIS DEGREE GRANTED Spring, 1983

Permission is hereby granted to THE UNIVERSITY OF ALBERTA LIBRARY to reproduce single copies of this thesis and to lend or sell such copies for private, scholarly or scientific research purposes only.

The author reserves other publication rights, and neither the thesis nor extensive extracts from it may be printed or otherwise reproduced without the author's written permission.

(SIGNED) Calvin W Domier

PERMANENT ADDRESS:

11759 - 37 Ave

Edmonton, Alberta

Canada

DATED April 3 1983

THE UNIVERSITY OF ALBERTA

FACULTY OF GRADUATE STUDIES AND RESEARCH

The undersigned certify that they have read, and recommend to the Faculty of Graduate Studies and Research, for acceptance, a thesis entitled Image Analysis as a Diagnostic Aid in Laser Research submitted by Calvin Wayne Domier in partial fulfilment of the requirements for the degree of Master of Science.

R. D. Hamburger
.....

Robert Tedosejevs
.....

Supervisors

W. A. Davis
.....

Date March 30, 1983

ABSTRACT

An optical data acquisition and processing system has been assembled and used to determine the spatial and spectral characteristics of a krypton fluoride (KrF) discharge laser system. The imaging system is composed of a vidicon camera, a 256 × 256 × 8-bit video digitizer system with its own internal video memory, and a 16-bit microcomputer system for analysis.

Software has been developed to allow the user to analyze the spatial profile of a laser beam, or to examine interference fringes that appear upon passing laser light through a Fabry-Perot interferometer and hence determine the laser linewidth. These image analysis routines have been incorporated into a master control program which can fire the laser, analyze the digitized images from the vidicon camera, monitor the timing of various components of the KrF laser chain and display energy readings obtained from a number of photodiodes and calorimeters.

The system has been used to characterize the spatial and spectral properties of a krypton-fluoride (KrF) discharge laser system. Resolution of the laser spectra was achieved with an ultraviolet Fabry-Perot interferometer, whose interference patterns were imaged onto the surface of a vidicon camera.

ACKNOWLEDGEMENT

This work was carried out in the Department of Electrical Engineering of the University of Alberta under the joint supervision of Dr. A.A. Offenberger and Dr. R. Fedosejevs.

Particular thanks are due to Dr. D.C.D. McKen and Dr. I.V. Tomov for their considerable help and direction in the laboratory portion of the work done, as well as guidance in determining the form that the computer analysis should take.

In recognition of the excellent technical support which has been received, I would also like to thank the following people: Mark Arnfield and Brian Betts for their considerable help in the laboratory; Herb Gans for his fine machining work in the EE machine shop; and Barry Arnold who provided high quality optics.

The author is thankful for the receipt of two years' National Sciences and Engineering Research Council of Canada Postgraduate Scholarship during the course of his studies.

Table of Contents

Chapter Page

1. INTRODUCTION 1
2. BACKGROUND AND THEORY 5
   - 2.1 Raman Pulse Compression 5
   - 2.2 Interference 7
     - 2.2.1 Two-beam Interference 7
     - 2.2.2 Multiple-beam interference 8
     - 2.2.3 Fabry-Perot Interferometer 11
   - 2.3 UV Imaging Techniques 17
   - 2.4 Analysis Requirements 19
     - 2.4.1 Hardware 19
     - 2.4.2 Software 21
3. EXPERIMENTAL 23
   - 3.1 KrF Laser System 23
   - 3.2 Fabry-Perot system for spectral analysis 26
   - 3.3 Data Acquisition System 28
     - 3.3.1 Video digitizer and video memory 28
     - 3.3.2 Microcomputer 31
     - 3.3.3 Hand-programming interface unit 32
     - 3.3.4 Printer 33
     - 3.3.5 Vidicon camera 33
   - 3.4 Imaging System 34
4. RESULTS AND DISCUSSION 38
   - 4.1 Calibration 38
   - 4.2 Spatial measurements 43
   - 4.3 Spectral measurements 48

4.4 Discussion 56
5. CONCLUSIONS AND RECOMMENDATIONS FOR FURTHER WORK 57
REFERENCES 60
APPENDIX 1. HAND-TOGGLE PROGRAMMING UNIT 62
APPENDIX 2. "ANALYZE" USER'S MANUAL 66

List of Figures

2.1 Schematic representation of stimulated backward wave Raman pulse compression. 6

2.2 Multiple beam fringes: ratio I_t / I_i as a function of phase difference δ. 10

2.3 Fabry-Perot interferometer. 12

2.4 Fabry-Perot interferometer (a) illuminated from an extended source, and (b) illuminated from a point source. 14

2.5 Fabry-Perot non-localized fringes in transmitted light: ratio I_t / I_i as a function of phase difference δ and $p(t/L)$. 15

2.6 Fabry-Perot non-localized fringes in transmitted light: peak transmission and FWHM linewidth in orders as a function of $p(t/L)$. 16

3.1 KrF laser system. 24

3.2 Transmission curves of angle tuned etalons E1, E2 and E3. 25

3.3 Data acquisition system. 29

3.4 Fluorescent emission spectrum of sodium salicylate. 36

4.1 Calibration geometry. 40

4.2 Transfer function of vidicon camera. 42

4.3 Spatial profile of the KrF laser beam (a) before processing, and (b) after processing. 46

4.4 Energy density histogram of the sampled KrF laser beam. 47

4.5 The output of a Fabry-Perot interferometer of the KrF laser controlled by (a) 2 angle-tuned etalons E_1, E_2 and (b) 3 angle-tuned etalons E_1, E_2 and E_3. 52

4.6 Horizontal scan through the centre of the fringe pattern of Figure 4.5(a). 53

4.7 Horizontal scan through the centre of the fringe pattern of Figure 4.5(b). 54

1. INTRODUCTION

In laser-pellet-fusion a small pellet of solid D-T fuel is irradiated from all directions by pulsed beams of laser light, where D and T are atoms of deuterium (^2H) and tritium (^3H) respectively. This energy is absorbed by inverse bremsstrahlung and resonance absorption processes at the critical layer $n_c = m\omega^2/4\pi e^2$, where $\omega = 2\pi c/\lambda$ is the frequency of the laser light, $m = 9.11\times10^{-28}$ g is the mass of an electron and $e = 1.60\times10^{-20}$ e.m.u. is the electronic charge[1]. A plasma shell forms on the surface of the pellet, which expands as the shell is heated. The momentum of the expanding shell is used in a rocket-like reaction to compress the central core of the pellet to the point where fusion then occurs[2].

The two laser systems that have received the greatest amount of attention as laser-fusion drivers have been Nd:glass (1.06 μm) and CO_2 (10.6 μm), due chiefly to the high power levels that have been achieved with these systems[3,4]. The current trend in laser-fusion, however, is toward shorter wavelength lasers with a higher value of n_c. Important advantages of short wavelength vs. long wavelength irradiation include increased absorption efficiency, reduced conversion of laser light to suprathermal electrons which preheat the core, and increased hydrodynamic compression efficiency[5].

With the shorter wavelength, however, there is an increased need for a more spatially uniform laser beam with

which to irradiate the target. As the wavelength decreases, so does the distance between the ablation and absorption surfaces of the target which greatly increases the effect of perturbations in the laser beam profile. It is for this reason that the spatial characteristics of the laser beam must be monitored.

Of the short wavelength lasers that have been proposed, the most promising have been the ultraviolet excimer lasers. The idea of the bound-free excimer laser system was first discussed in 1960 by Houtermans. The term *excimer* was borrowed from organic photochemistry where it had been used as a contraction for an excited dimer. It is now used to describe any molecular laser with a dissociative lower laser level. Although the rare gas halide lasers weren't discovered until 1975, they are presently the most highly developed of all the excimer lasers. The krypton flouride (KrF) laser, with a wavelength of 248 nm, has shown promise to be efficient and scalable to high energy per pulse[6].

Unfortunately, the excimer lasers suffer from the problem of having low energy storage, which is a disadvantage for some applications (notably laser fusion). This is due to the short lifetime of the upper laser level (few ns) and the high stimulated emission cross-section (10^{-14} cm^2). Excimer lasers must therefore store energy in the form of a beam of photons, hence the energy of the excimer laser increases with longer pump times. In order to generate the very short pulses (less than 10 ns) of high

energy that are needed for use as a laser-fusion driver special techniques must be employed, such as beam splitting, delaying, amplifying and stacking of pulses[7]; using stimulated Raman scattering (SRS) to extract the energy in a long pulse by counter-propagating a Stokes shifted probe pulse of the desired pulse length[8]; or using a hybrid of the two techniques[9].

To achieve efficient backward Raman compression a spectrally narrow pump pulse is required. The Raman gain is highly dependent on the linewidth of the pump pulse and a spectrally broad pump pulse generates no backward radiation irrespective of the intensity of the pump pulse[10]. Thus the need exists for a spectral monitor on the laser beam as well.

In order to determine the spatial and spectral characteristics of the KrF laser beam, an optical data acquisition and processing system was therefore assembled. This system was composed of a vidicon camera, a 256×256×8-bit video digitizer system, and a 16-bit microcomputer for analysis. To generate the narrow linewidth needed for efficient Raman compression, a stack of 3 angle-tuned etalons had to be designed for use with the KrF oscillator. Linewidth measurements were made with the aid of a Fabry-Perot interferometer.

In Chapter 2, the background and theory of Raman pulse compression is discussed. A study of the Fabry-Perot interferometer is made, following a review of relevent

interference theory. Different methods of imaging ultraviolet light are examined and a list of hardware and software requirements of the analysis system is provided.

Chapter 3 contains descriptions of the experimental KrF laser system, including the line-narrowing etalons, and outlines the procedure used to align the Fabry-Perot interferometer. The data acquisition and imaging systems are discussed.

A general discussion of experimental results is given in Chapter 4. The steps taken to calibrate the imaging system are cited and the results of these calibration tests are described. Some sample laser shots are analyzed both spatially and spectrally and the measurements are discussed. Finally, the strong and weak features of the system are stated.

Chapter 5 summarizes what has been accomplished with the system to date and describes a number of improvements to the system which could be implemented at a later date.

Appendix 1 describes the hand-programming unit in some detail and includes circuit schematics of the unit. Appendix 2 contains the user's manual to the program *ANALYZE*, which has been developed to handle all the optical data acquisition and processing needs. This manual describes how the program is used, as well as a description of many of the routines used.

2. BACKGROUND AND THEORY

2.1 Raman Pulse Compression

The principle on which backward Raman pulse compression operates is shown in Figure 2.1. A long laser pump pulse propagates from right to left through a Raman medium, producing gain at the first Stokes frequency $\nu_m = \nu_p - \nu_s$, where ν_p is the pump frequency and ν_m is the frequency of the Raman mode that has been excited. Just as the pump pulse reaches the exit window, a shorter pulse at frequency ν_s is injected into the cell in the opposite direction. As the two pulses move through one another, the Stokes pulse grows at the expense of the pump pulse. The net result is that the long pulse at ν_p is compressed into the short pulse at ν_s.

Murray et. al.[11] have reported on some work on Raman compression of KrF laser light in methane. The Stoke's pulse was produced by superfluorescence from the pump wave. They have shown that the backward Raman gain is approximately described by

$$g = \exp\left\{\frac{\lambda^2 P}{h\nu_p \pi(\Delta\nu_p + \Delta\nu_m)}\right\} \frac{\partial\sigma}{\partial\Omega} \int I_p \, dl, \qquad (2.1)$$

where P is the density of scatterers, $\frac{\partial\sigma}{\partial\Omega}$ is the differential scattering cross section, I_p is the pump laser intensity and the integral extends over the length of the cell. Furthermore, $\Delta\nu_p$ and $\Delta\nu_m$ are the HWHM (half-width half-maximum) linewidths of the pump laser and the Stokes

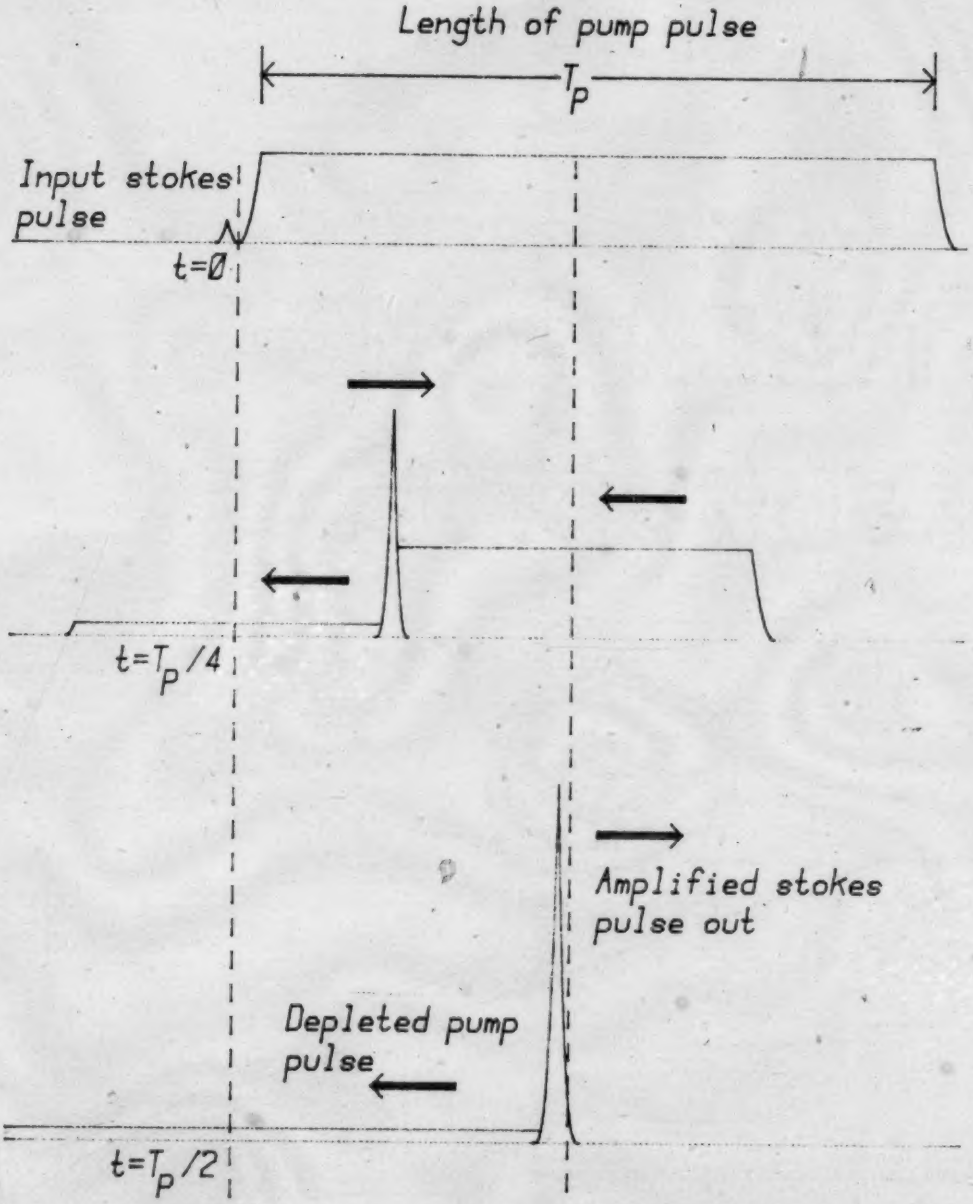


Figure 2.1 Schematic representation of stimulated backward wave Raman pulse compression.

medium respectively. Note that for methane, $\Delta\nu_m$ is approximately constant over the pressure range from 1-10 atmospheres and has the value $\Delta\nu_m \sim 0.15\ cm^{-1}$. Thus the gain is highly dependent on the laser linewidth, until the linewidth of the laser has fallen below the linewidth of the medium.

2.2 Interference

One of the most accurate techniques for linewidth measurement uses optical interference phenomena, in particular, Fabry-Perot systems. In addition, optical interference can be used in narrowing the laser linewidth. It is therefore useful to review the theory behind optical interference.

2.2.1 Two-beam Interference

When two or more beams of light are superimposed, the intensity in the area of superposition can vary between maxima which exceed the sum of the individual beam intensities, and minima which can be zero. This phenomenon is known as *interference*. Consider first the case of two light waves of intensity I_1 and I_2 propagating in the same direction. The total intensity is then given by

$$I = I_1 + I_2 + 2\sqrt{I_1 I_2}\cos\delta, \qquad (2.2)$$

where δ is the phase difference between the two beams. Obviously there will be a maximum of intensity

$$I_{max} = I_1 + I_2 + 2\sqrt{I_1 I_2}$$

when $|\delta| = 0, 2\pi, 4\pi, \ldots,$ (2.3)

and a minimum of intensity

$$I_{min} = I_1 + I_2 - 2\sqrt{I_1 I_2}$$

when $|\delta| = \pi, 3\pi, \ldots$ (2.4)

2.2.2 Multiple-beam interference

When a beam of light is incident on a transparent parallel plate with both sides having high reflectivity coatings, there are multiple reflections at the plate surfaces. Suppose now that the parallel plate has thickness t and refractivity μ, and let a plane wave of wavelength λ be incident on the plate at an angle θ. Between consecutive beams, the optical path difference will be $2\mu t\cos\theta$ or a phase difference of

$$\delta = (2\pi/\lambda)\, 2\mu t\cos\theta. \quad (2.5)$$

Let A_i be the complex amplitude of the electric vector of the incident wave. Furthermore, let R and T be the reflectivity and transmissivity of the plate surfaces respectively, which are related by

$$R + T = 1. \quad (2.6)$$

The amplitude A_t of the transmitted light due to the superposition of the first p reflections is:

$$A_t(p) = T(1 + Re^{i\delta} + \ldots + R^{(p-1)}e^{i(p-1)\delta})A$$

$$= \left[\frac{1 - R^p e^{ip\delta}}{1 - Re^{i\delta}}\right] TA_i \quad (2.7)$$

which, as $p \to \infty$, reduces to

$$A_t = TA_i/(1 - Re^{i\delta}). \qquad (2.8)$$

The corresponding intensity $I_t = A_t A_t^*$ of the transmitted light is then given by:

$$I_t = \frac{T^2 I_i}{1+R^2-2R\cos\delta} = \frac{T^2 I_i}{(1-R)^2+4R\sin^2(\delta/2)} . \qquad (2.9)$$

This formula is known as *Airy's formula*, and may be rewritten using (2.6), as

$$I_t = \frac{I_i}{1 + F \sin^2(\delta/2)} \qquad (2.10)$$

where the *measure of sharpness* F is defined by

$$F = \frac{4R}{(1-R)^2} . \qquad (2.11)$$

The FWHM (full-width half-maximum) linewidth W is readily calculated from (2.10). If the fringes are sharp enough that the half-width can be replaced with its sine, then W as a fraction of an order is

$$W = \frac{\Delta\lambda}{\lambda} = \frac{2}{\pi\sqrt{F}} = \frac{1-R}{n\sqrt{R}} . \qquad (2.12)$$

Another useful measure is the *finesse* F of the system, where $F = 1/W = (\pi\sqrt{R})/(1-R)$.

The behaviour I_t/I_i as a function of the phase difference δ is shown for various values of R in Figure 2.1. Note that as $R \to 1$, the pattern consists of narrow bright fringes on an almost almost totally dark background.

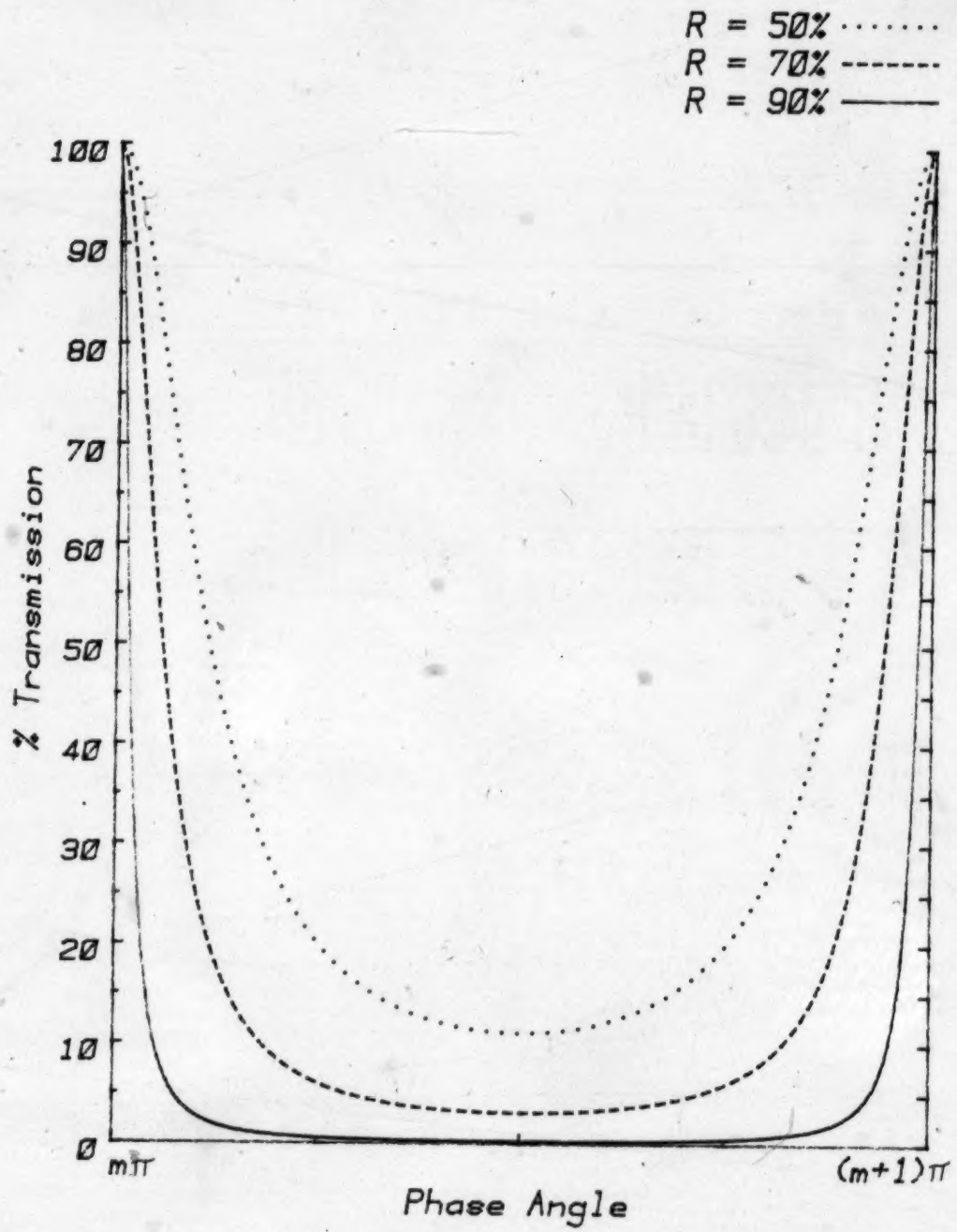


Figure 2.2 Multiple beam fringes: ratio I_t/I_i as a function of phase difference δ.

2.2.3 Fabry-Perot Interferometer

The Fabry-Perot interferometer is composed of two quartz plates as shown in Figure 2.3. The outer surfaces are wedged at ~ 30 minutes of arc, away from the highly reflective inner surfaces so as to avoid unwanted reflections at the outer uncoated surfaces. The back plate is mounted on a dove-tailed railing perpendicular to the housing and can be moved linearly to permit a spacing of up to 20 cm. The front plate, which is fixed in place, can be adjusted angularly with the aid of two micrometers mounted in the chassis to align it perpendicular to the back plate.

The Fabry-Perot interferometer is usually placed in one of two configurations. In the standard set-up, as shown in Figure 2.4(a), the rays which interfere at a point are parallel and form rings at angular positions θ given by $n\lambda = 2\mu t\cos\theta$. Let n_o be the order of interference at the centre of the ring pattern ($\cos\theta = 1$), then

$$n = n_o\cos\theta. \qquad (2.13)$$

The bright fringes, which correspond to integral values of n, are circles with a common centre at the focal point. The fringes follow the standard Airy distribution shown in Figure 2.2 and appear only over the region covered by the image of the source. Using the cosine expansion, $\cos\theta = 1 - \theta^2/2$, Born[12] has shown that the angular radius of the pth ring is approximately given by

$$\theta_p = \sqrt{(p-1+\epsilon)\lambda/t}, \qquad (2.14)$$

where ϵ is the fractional order at the centre and the medium

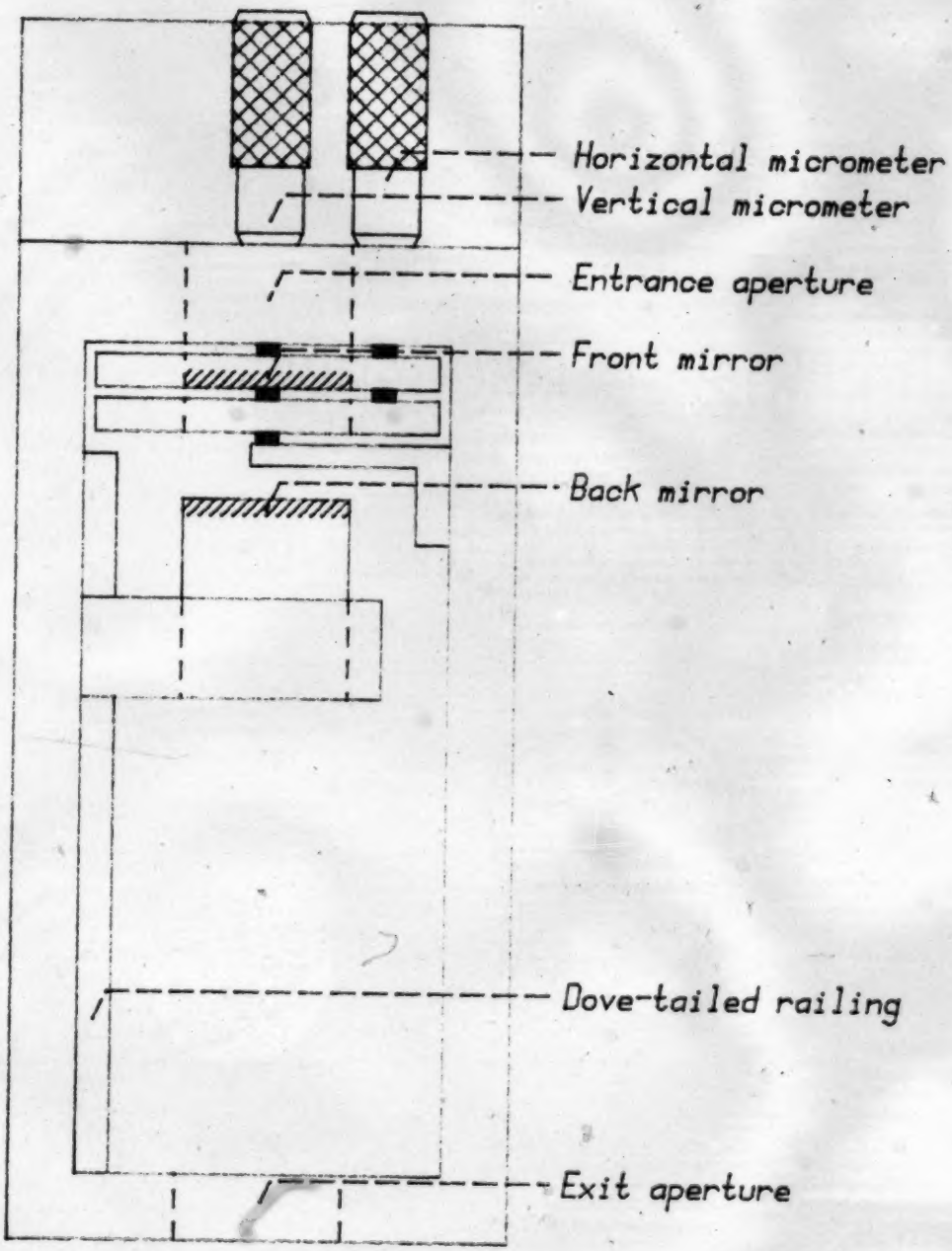


Figure 2.3 Fabry-Perot interferometer.

has refractivity $\mu=1$ (i.e. air). The diameter D_p of this fringe is then given by $D_p = 2f\theta_p$, where f is the focal length of the lens L_2. These fringes are referred to as *localized* because they only appear at the focus of the lens L_2.

In the alternate configuration shown in Figure 2.4(b), the fringes diverge in cones from the source and extend outwards from the interferometer into space and are hence referred to as *non-localized*. In this case the rings become larger as the screen is taken farther away from the source. The diameter D_p of the pth ring is $2L\theta_p$, where L is the distance from the source S to the screen. From (2.14) this may be rewritten as

$$D_p = 2L\sqrt{(p-1+\epsilon)\lambda/t}. \qquad (2.15)$$

One advantage of this configuration is that it allows the screen to be tilted with respect to the beam path, with the image suffering only a geometrical distortion.

The theory of the ring formation is as follows. As a result of multiple reflections, the effect at a point P upon a screen located a distance L from a source S is equivalent to that produced by a series of point-sources S, S_1, S_2, S_3, ... , each a distance $2t$ apart. The path difference between the two rays from S and S_n can be written as:

$$D_n = \sqrt{y^2+[L+2nt]^2} - \sqrt{y^2+L^2}, \qquad (2.16)$$

where y is the distance from the centre of the fringe pattern to the point P. Tolansky[13] has shown that, for $L >> t$, D_n is approximately given by

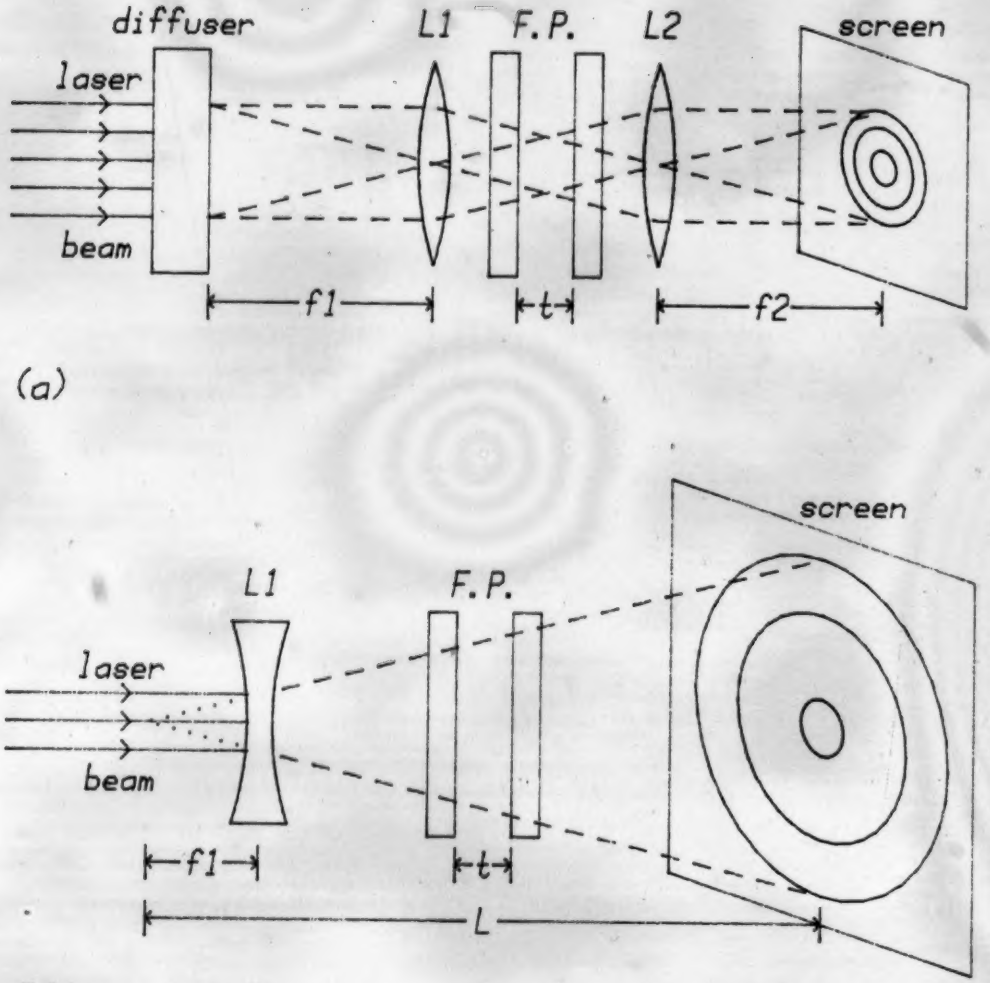


Figure 2.4 Fabry-Perot interferometer (a) illuminated from an extended source, and (b) illuminated from a point source.

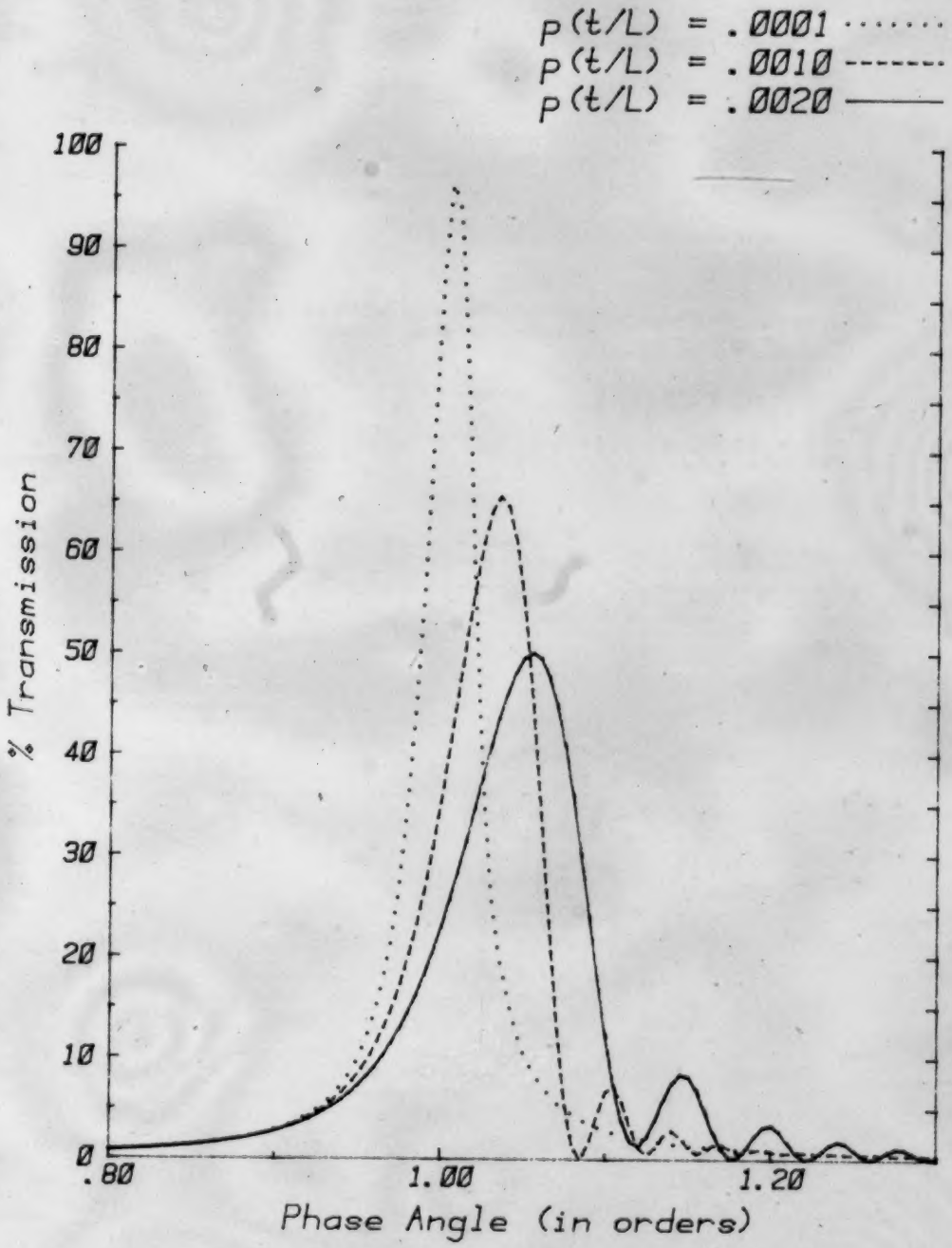


Figure 2.5 Fabry-Perot non-localized fringes in transmitted light: ratio I_t/I_i as a function of phase difference ó and $p(t/L)$.

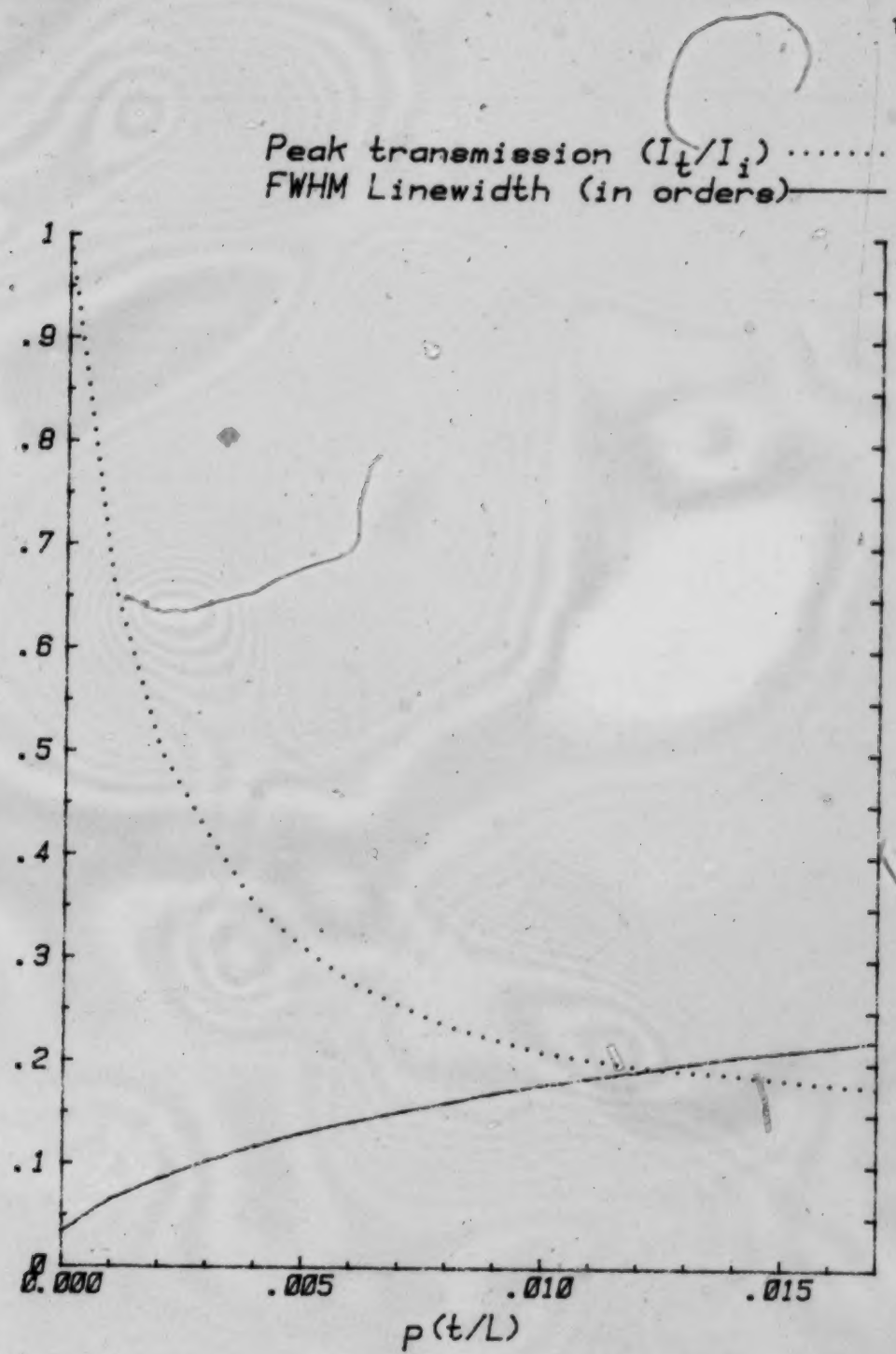


Figure 2.6 Fabry-Perot non-localized fringes in transmitted light: peak transmission and FWHM linewidth in orders as a function of $p(t/L)$.

$$D_n = 2nt\cos\theta + 2n^2(t^2/L)\cos\theta\sin^2\theta, \qquad (2.16)$$

where only first order terms in t/L have been kept. He goes further to state that if t/L is kept below some limiting factor, say 10^{-4}, there is an almost complete Airy distribution.

Using instead the exact expressions, the intensity distributions I_t/I_i have been calculated for a number of different values of $p(t/L)$ and are shown in Figure 2.5 for the case when λ = 248 nm and the reflectivity of the etalons is 90%. Instead of the symmetrical arrangement that is a result of the first F.P. arrangement, an asymmetrical fringe pattern appears, with secondary fringes on the outside of each ring. The peak intensity is found to decrease and the FWHM linewidth increase as the factor $p(t/L)$ gets larger, i.e. as one looks at fringes of higher order away from the central spot, as is illustrated in Figure 2.6.

2.3 UV Imaging Techniques

One of the most commonly used methods of analyzing u.v. laser light is to form an image on u.v. sensitive paper; one such type commercially available is called *Dylux paper*. This paper undergoes an instantaneous color change from yellow to blue upon exposure to ultraviolet rays with intensities in the range 1-200 mJ/cm^2, thus providing a low contrast but inexpensive way of examining the laser light. After a few hours' exposure to room light the paper sets, at which point

the paper has turned completely blue (the shade of blue is dependent on the laser intensity to which it has been exposed). In order to translate the shades into an accurate record of the laser intensity, however, would require making 2D optical density measurements of the beam image. As this is a time consuming process, it is ill-suited for real-time laser diagnostic work.

As an alternative, a simple photo-emulsion (i.e. an undeveloped photograph) could be placed in front of the beam. When exposed to light, the density of the photo-emulsion formed is directly proportional to the integrated light intensity that the photograph has been exposed to. The resultant photograph, which has an intrinsically higher contrast than u.v. sensitive paper, can be analyzed using a photodensitometer. Unfortunately this too is a slow and inconvenient process that does not satisfy the needs of a real-time diagnostic system.

A two-dimensional array of light sensitive detectors, or equivalently a vidicon camera, has a dynamic range comparable to that of the photograph. When combined with a video digitizing system and a computer for immediate processing, it can provide real-time analysis of the laser beam on a shot-by-shot basis. It would be preferable to use a u.v. sensitive vidicon, but in the absence of such an instrument a system composed of a visible light vidicon focussed on a scintillator screen could be used. This in fact was the method employed due to the unavailability of

u.v. vidicons.

2.4 Analysis Requirements

After assessing the experimental requirements, a detailed list of desired hardware and software features was determined to achieve the desired combination of high resolution, high dynamic range image gathering and real-time image processing and analysis.

2.4.1 Hardware

To be useful as a laboratory diagnostic tool, it was decided that the video digitizer used should have a resolution of at least 256×256 pixels (picture elements) with a minimum grey scale of 6 bits/pixel. It must be able to digitize an entire video image within a single video frame (16.67 ms), and should include sufficient memory to store the full image. The unit should generate a standard NTSC video signal from the stored image to directly drive low cost colour or black and white TV monitors. The capability of both reading and writing individual pixels and/or groups of pixels must also be present.

A 16-bit microcomputer was deemed necessary to analyze the raw data. The computer should be a multi-user system, with the capability of running in a real-time mode (i.e. to temporarily turn off all other users to allow for real-time data gathering). Language support should include Fortran 77

and C. Another additional requirement was due to the laboratory's prior commitments to the purchase of other diagnostic equipment which operate from a CAMAC bus structure. Interfacing was commercially available between the CAMAC bus and and the Multibus, PDP-11 bus and LSI-11 bus structures; therefore the microcomputer, as well as the video digitizing system, should be compatible with one of the three bus architectures.

A video camera is needed which is compatible with the video digitizer system. As most cameras do not respond to ultraviolet light, there is the added problem of how to image the 248 nm light of the KrF laser. The first choice would be a camera whose response curve extends far enough into the far ultraviolet to be directly useful in this application, however these cameras tend to be exorbitantly expensive. Alternatively, one could direct the laser light to a scintillator screen which absorbs the ultraviolet light and re-emits this energy in the form of visible light which can be subsequently detected by a camera focused on the screen.

Additional hardware needs include a video monitor and some sort of hard-copy unit such as a printer. Although the primary purpose of the printer would lie in the generation of program listings, the ability to do graphics would be a definite asset. In addition, the computer must be provided with some means of triggering the laser.

Finally, the equipment should be shielded from electrical noise. As the KrF laser modules are all driven by high voltage spark gaps, the electrical interference that this produces is considerable. This necessitated placing all of the diagnostic equipment inside a screened room, with the camera being the only piece of equipment that lies in the unshielded laboratory environment.

2.4.2 Software

The analysis program should be menu-driven. In command mode, all command options should respond to a single keystroke. After triggering the laser, it must digitize the video image from the camera and assemble the data from the CAMAC units. All other analysis operations must be specifically requested after having returned to command mode.

Spatial analysis should determine the maximum and minimum values, compute the mean and the standard deviation about the mean and compute the amount of energy present in the laser beam. If possible, it should also compute a histogram of the energy levels and display the histogram on the user's terminal.

Spectral analysis should determine the maximum and minimum values and the background light level. It should correct the fringe pattern for any variations due to spatial non-uniformities in the beam and compute the linewidth of the laser beam. If possible, it should also display the

laser's spectral profile on the terminal. Finally, it should compute the percentage injection, i.e. the percentage of the laser beam's energy that has been successfully injected into the single line which makes up the fringe pattern shown on the screen. Obviously if the percentage injection is low then most of the beam is composed of broadband laser light which cannot be used for efficient Raman pulse compression.

3. EXPERIMENTAL

3.1 KrF Laser System

The KRF discharge laser system, as shown in Figure 3.1, is similar to that developed at Lawrence Livermore National Laboratory[7] and is reported elsewhere[9,14]. The master oscillator is a stable resonator composed of a concave (r_1 = 4m) 100% reflecting mirror M_1 and a flat 90% reflecting mirror M_2, and has 30 cm of active gain length. The injection-locked amplifier is an unstable resonator composed of the flat mirror M_2 and a convex (r_3 = 0.6m) 2 mm diameter meniscus mirror M_3, with a one meter discharge length. By placing a 5 m focal length lens L_1 at a distance of 1.52 m from M_3, a beam with a divergence about three times the diffraction limit is formed.

The oscillator bandwidth is controlled by three angle tuned etalons E_1, E_2 and E_3 which are an air-spaced 0.1 mm gap and solid 0.5 mm and 3.0 mm fused silica flats respectively. All were coated for 75% reflectivity at 248 nm. Each etalon can be considered as an interferometer which filters the laser light by wavelength. From (2.4) the peak transmission occurs for $m\lambda = 2\mu t\cos\theta$, where μt is the optical thickness of the etalon in question. The transmission curves of the etalons are shown in Figure 3.2.

When properly adjusted only a single transmission peak, whose passband is 0.2 cm^{-1}, is above the threshold for

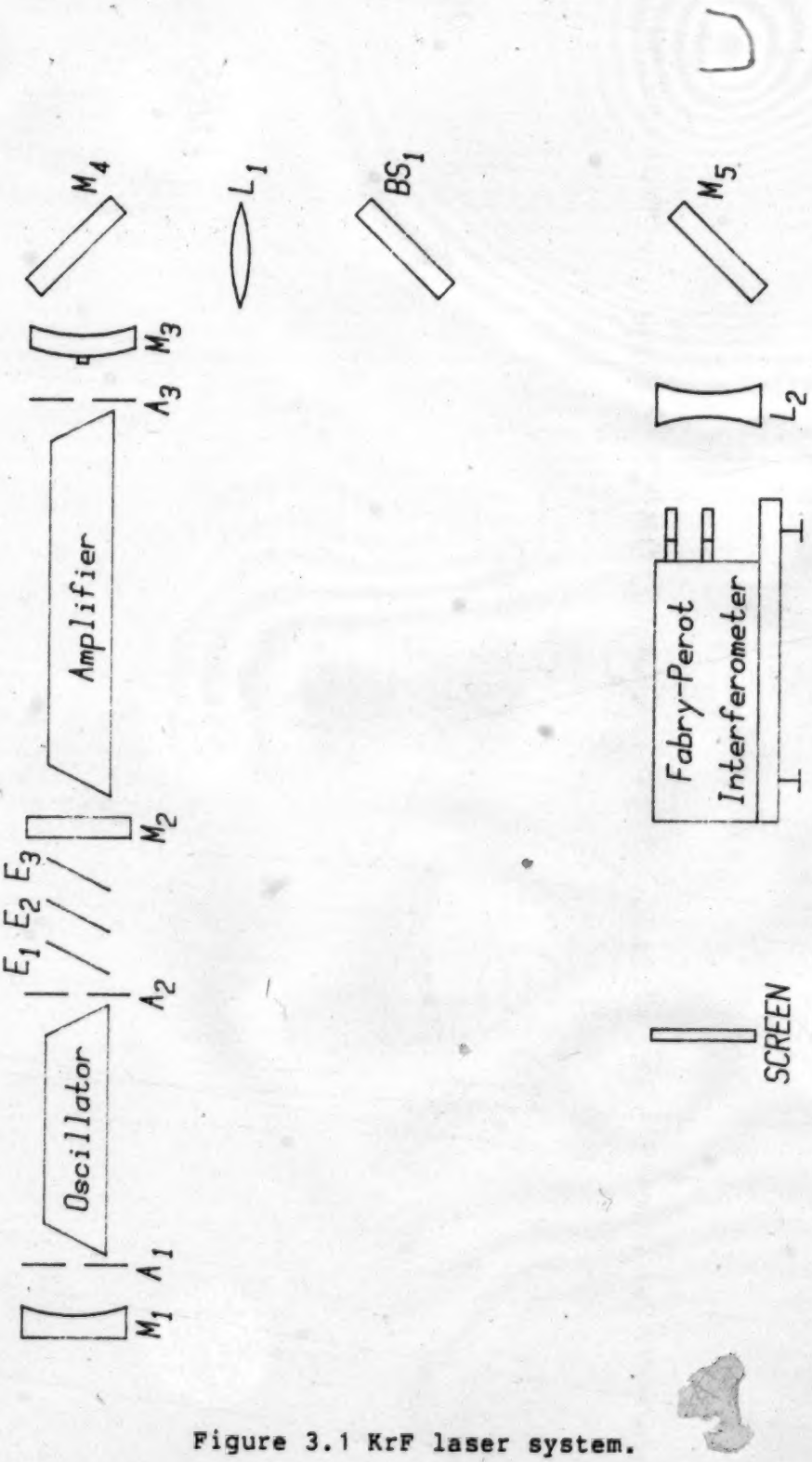


Figure 3.1 KrF laser system.

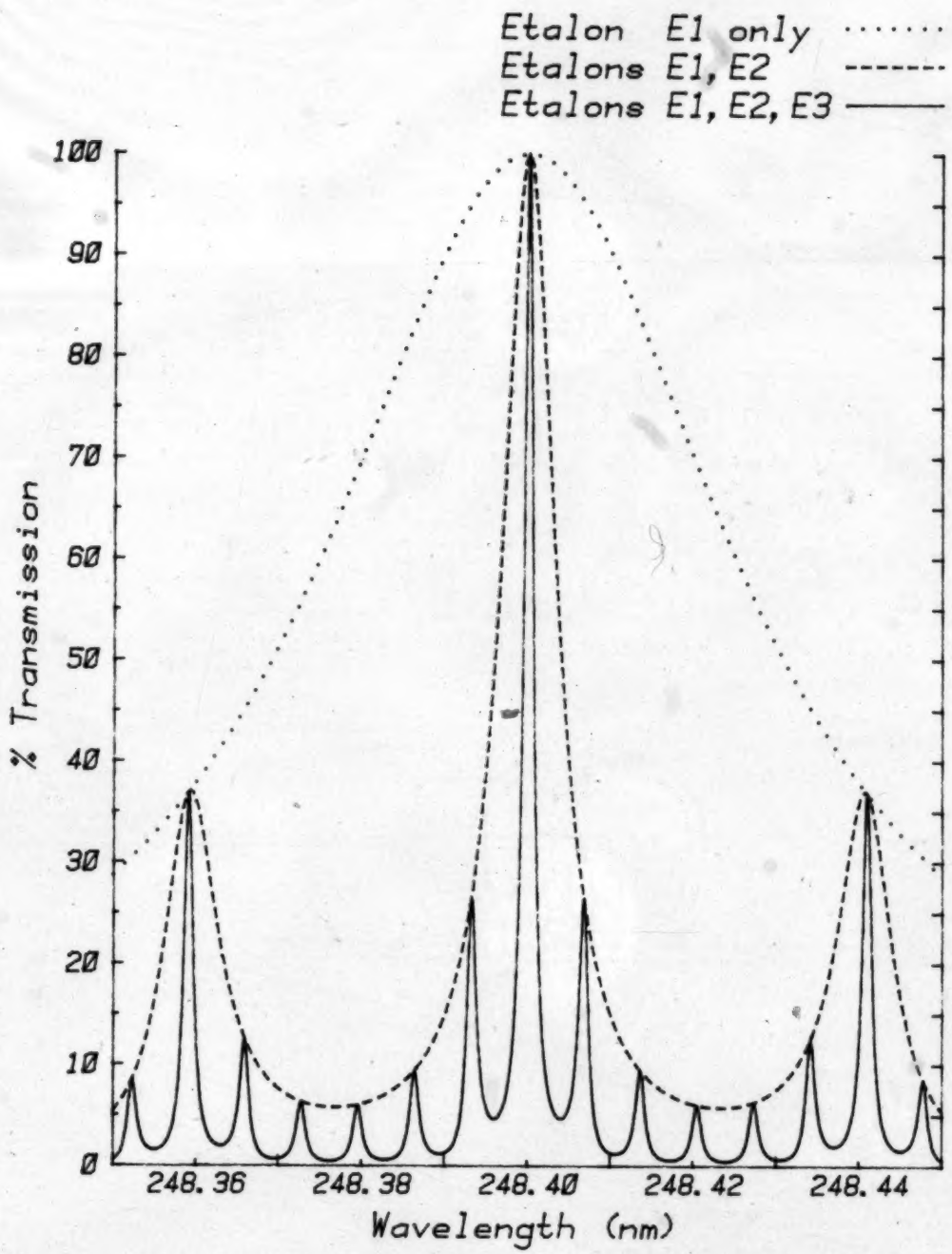


Figure 3.2 Transmission curves of angle tuned etalons E1, E2 and E3.

lasing. With multiple round trips through the oscillator during the buildup of the pulse, the output linewidth is narrowed to less than 0.1 cm^{-1}. The aperture A_1, set at 2 mm diameter, controls the transverse mode quality while the aperture A_2, set at 4 mm diameter, blocks the reflected light signals from the etalons. The aperture A_3 sets the size of the output beam.

The master oscillator produces an output of 0.2 mJ in a 25 ns pulse when operating with a fresh laser gas fill of 28 psia. The injection-locked slave oscillator produces a uniform beam with a cross-sectional area of ~ 8 cm^2 and up to 400 mJ in a 25 ns (FWHM) pulse. The pump pulse is then passed through a beam splitter *BS*, which directs about 90% of the pulse energy to laboratory experiments and the rest is directed via a flat 100% reflecting turning mirror *M*, to a Fabry-Perot interferometer for spectral analysis.

3.2 Fabry-Perot system for spectral analysis

The Fabry-Perot cavity is composed of two plano mirrors of high reflectivity, aligned parallel to each other and perpendicular to the incoming light. The Fabry-Perot interferometer used for these experiments is composed of one fixed mirror and one adjustable mirror and has been described in section 2.3.3 (see Figure 2.3). These mirrors were specially prepared for use with ultraviolet light and have a maximum reflectance of 90% at 250 nm, giving a

finesse F = 30. The reflectivity remains high enough at 623 nm, however, to allow the system to be aligned with a cw He-Ne laser.

The initial alignment is done with a cw He-Ne laser which has been lined up to follow the same optical path as the KrF laser. The first step is to place the interferometer perpendicular to the beam, by adjusting its position until the He-Ne light is centred on the entrance and exit apertures. This guarantees that the laser beam and the back mirror are perpendicular to better than 0.2°. Next, expansion optics are placed in front of the Fabry-Perot providing the divergence to produce interference patterns in the output beam. The expansion optics then have to be adjusted so that the beam passing through is once again centred on the entrance aperture.

The final alignment of the Fabry-Perot has to be done with the KrF laser itself. A flourescent card is placed after the interferometer, enabling the fringes to be seen on its surface. If at this point the two mirrored surfaces of the Fabry-Perot are at a slight angle to one another, the fringe pattern will appear but will be off-centred. The front etalon is then adjusted until the fringe pattern is centred on the card. At this point the Fabry-Perot system has been fully aligned, with the mirrors parallel to each other and perpendicular to the KrF laser beam.

3.3 Data Acquisition System

The laser diagnostic system that was developed consisted of the following components:

1. video digitizer and video memory,
2. 16-bit microcomputer,
3. hand-programming interface unit,
4. dot-matrix graphics printer,
5. video camera.

3.3.1 Video digitizer and video memory

The video digitizer system that was finally chosen was one offered by MATROX Electronic Systems Ltd. which consisted of the following items:

1. one FG-01/8 8-bit frame grabber card,
2. two RGB-256 video memory boards,
3. one CCB-7 Multibus chassis and back plane.

The Matrox cards plug directly into IEEE 796 Multibus, although equivalent versions of the same cards are available in both PDP-11 and LSI-11 bus structures. The 7-slot CCB-7 Multibus cardcage and back plane was bought to house the video cards and provide extra slots for future expansion.

The FG-01 is a high speed analog to digital converter card. The card permits the user to digitize a standard monochrome video signal (1V p-p) and write the digitized video field into the RGB-256 display refresh memory. As each RGB-256 card features a 256×256 dot resolution with 4 bit planes, two RGB-256 cards have to be combined to store the

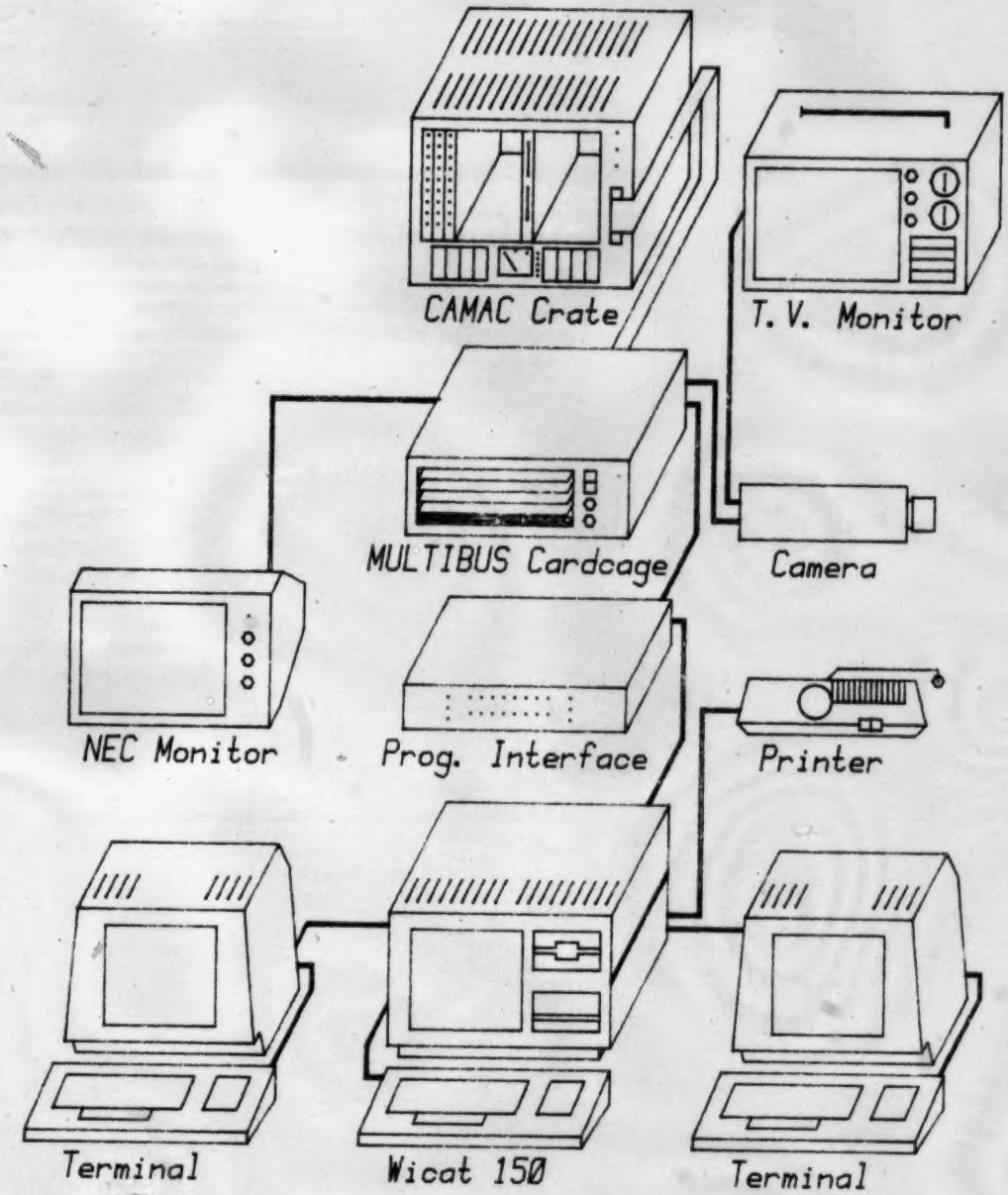


Figure 3.3 Data acquisition system.

full 8 bits/pixel that the FG-01/8 provides.

The system from MATROX provides software-controlled frame-grabbing on any of four camera inputs in 16-32 ms. The image memory is fully addressable, with read and write pixel commands taking only 1.4 μsec. A built-in scroll register allows the display to be shifted vertically with a one line resolution. Additional features include built-in NTSC color and grey scale encoders which give a total of 256 colors or grey levels.

The FG-01 board also permits the system to be connected to other microcomputers or minicomputers via an external interface. On-board circuitry allows the external computer to access any device in the Multibus I/O map through the FG-01 board. Thus the CAMAC crate controller card could be placed in the Multibus cardcage and be controlled by the other computer through the external interface.

The system is capable of being run in two different modes: master sync and slave sync. In the master sync mode, the video memory cards generate required sync signals internally and these signals are used to externally drive the various cameras. External sync, on the other hand, locks the video cards to the composite sync of the video output of the cameras, with an exact number of vertical and horizontal sync pulses needed for good locking of the two RGB-256 memory boards with each other.

3.3.2 Microcomputer

In order to fulfill the computing needs, a 16-bit WICAT 150 Multiuser System was purchased. At the heart of the system is an MC68000 16-bit microcomputer and 512 Kbytes of RAM (Random Access Memory), which is expandable to 12 Mbytes. Inside the system is an asynchronous 7 slot MULTIBUS, 5 of which were already filled when shipped out from the factory. Data storage is achieved via a 10 Mbyte 5 1/4" Winchester hard disk and a 616 Kbyte 5 1/4" floppy drive for backup. It contains a single parallel port and 6 serial RS-232 ports and can thus handle up to 6 terminal users simultaneously.

The operating system is UNIX-like, supporting a shell-like file structure, permitting directories and sub-directories. The software includes FORTRAN 77, C-programming language and an MC68000 assembler. Source files can be edited through the aid of a sophisticated visual editor.

At the time of writing this thesis, a bus-expander had not yet been developed for the Wicat to enable the main system bus to connect directly with other Multibus cardcages. This meant that only the 2 free slots left in the system bus were available for other Multibus boards. Since the MATROX imaging system alone needed three slots, the external interface of the FG-01 board was wired to a standard D-25 parallel port connector. Software was then written to permit the Wicat's parallel port to control the

cards in the external Multibus cardcage at some sacrifice of speed but with more isolation from electrical interference.

3.3.3 Hand-programming interface unit

For the purpose of testing the Multibus cards, as well as debugging the software routines that had to be written to communicate with said cards, a hand-toggle programming unit was assembled. This unit operates in conjunction with the external interface of the FG-01 in one of two modes: as a stand-alone unit it allows the user to toggle in read/write instructions directly; or as a buffer unit it relays those instructions from the Wicat.

Upon the conclusion of every read/write operation, each of the 16 address and data lines are latched and connected up to an LED (Light Emitting Diode), thus displaying the address and data bytes in bit-format. At the same time read, write and acknowledge LEDs flash to indicate the state of the respective control lines.

A method still had to be found to trigger the laser and the video digitizer simultaneously. Upon examination of the video digitizer board, a line was found on the board that goes low and stays low during a digitize or clear operation. The connection between the external interface and the hand-programming unit was then modified to pass this signal to the hand-programming unit, where it was used to send a 30 volt trigger pulse to the KrF laser. Thus whenever the command is given to digitize a video picture, the laser is

triggered automatically. Further details of this interface, as well as circuit schematics, are provided in Appendix 1.

3.3.4 Printer

To satisfy the need for hard-copy listings of programs, an EPSON MX-80 dot matrix printer with the GRAFTREX-80 high resolution graphics option was purchased. As the parallel port of the Wicat microcomputer was already used for communication with the external Multibus boards, a 2 Kbyte serial buffer interface for the printer was also bought to allow the printer to operate from one of the Wicat's 6 serial ports.

The printer is capable of writing 40, 66, 80 or 132 characters per line. In graphics mode, the printer can write up to 180 dots per inch horizontally and 72 dots per inch vertically. This high density graphics capability makes is possible to produce high density black & white pictures, or pseudo grey scale pictures in a reasonably swift and easy fashion.

3.3.5 Vidicon camera

For maximum flexibility, any camera chosen had to allow the video digitizer to operate in both sync modes. Although most cameras were found able to be externally synchronizeed, very few provided a composite video output with full NTSC standard sync signals with serrations which the MATROX boards require. The only standard vidicon cameras that were

tested and met these specifications were manufactured by RCA. These included two fibre-optically coupled cameras which were modified for ultraviolet use by attaching a scintillating material onto the surface of the vidicon tube. The original scintillator material provided was found to be inappropriate for the short 250 nm wavelength being used in these experiments, exhibiting poor sensitivity and very nonuniform response across the surface. This shortcoming, in addition to a thermal instability problem, rendered them unusable for the direct imaging of the KrF laser light as they were intended. Therefore, an interim solution comprising a scintillator screen and a high quality visible light 2/3" vidicon camera was found to perform satisfactorily.

3.4 Imaging System

In order to image the ultraviolet laser light, the light had to be directed to a flourescent screen which would absorb the uv-light and re-emit visible light; this fluorescence was then detected by the visible-light camera focused on the screen. Since the camera was to be scanned in a single T.V. frame (16.67 ms), any fluorescent screen used had to have a fast response time, preferably much less than 1 msec.

Two standard u.v. sensitive thin layer chromogram sheets made by Eastman Kodak were tested for their

applicability: an orange screen was found to have a lag time on the order of 15 msec; a green screen had a lag time of about 1 msec. The slow response time resulted in a distorted video output from the camera: those portions of the camera's sensing area that are first scanned show quite low light levels, while those portions that are scanned last register much higher light levels. The best response by far was obtained with a screen composed of sodium salicylate that was prepared in the lab.

Sodium salicylate emits at 420 nm, has a quantum efficiency of almost 90%, and has a fluorescent decay time of 10 nsec[15]. The sodium salicylate, which was obtained in powder form, was mixed with ethanol to form a saturated solution. This solution was poured onto the surface of the screen, and was then placed under a heat lamp and allowed to evaporate, leaving behind a powdery white residue. Two or three coatings proved sufficient to give a uniform density over the whole surface of the screen.

The first sodium salicylate screen was prepared on a 3 inch diameter glass plate. A vidicon camera was placed behind the interferometer, with the plate placed between them. The camera, focused onto the plate, imaged the flourescent light transmitted through the glass onto the surface of the vidicon. This set-up meant there was no distortion in the imaged picture, but it required high light levels. In addition, the image was blurred slightly due to the flourescent light having to pass through the full

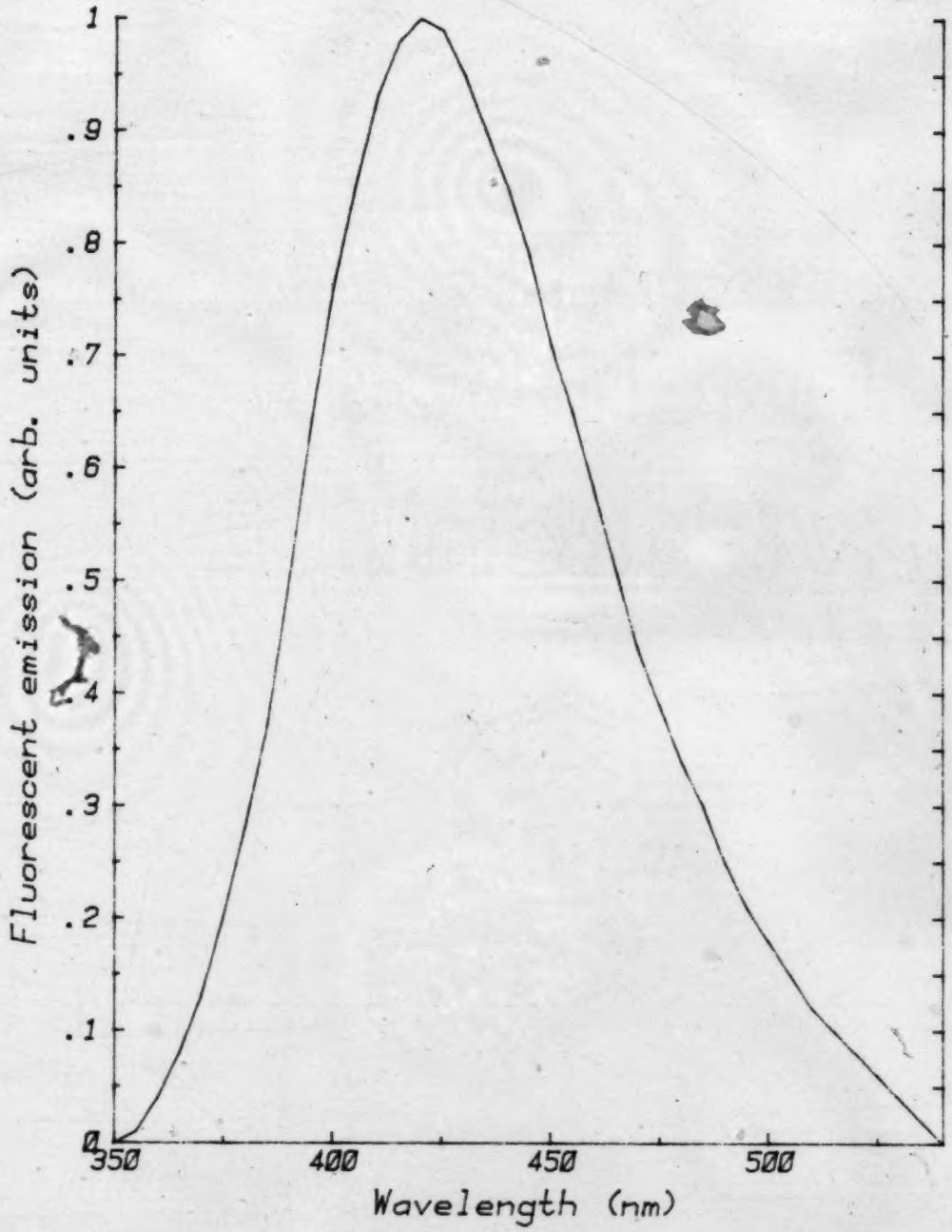


Figure 3.4 Fluorescent emission spectrum of sodium salicylate.

thickness of the scintillating material.

A second scintillator screen was then prepared on a 4" × 6" aluminium plate. This plate was mounted along with the camera on a triangular base and the whole assembly then placed in the output beam. In this set-up the camera is imaged on the front surface of the scintillator, thus reducing the input light level required for the camera. However, in order to image the beam onto the scintillator the camera/scintillator assembly had to be placed at an angle of about 25° to the normal, which distorted the viewed image by a similar amount.

4. RESULTS AND DISCUSSION

To have a quantitative measurement system, the following characteristics need to be determined:

(1) transfer function response as a function of pixel position x,y and the digitized pixel value P(x,y) at that point,

(2) pixel noise level,

(3) geometric distortion effects,

(4) resolution capability.

4.1 Calibration

Before the imaging system could be used for any scientific measurements, it had to be calibrated. This meant determining the transfer function of the camera/scintillator combination in order to convert the digitized pixel values P(x,y) into integrated intensity values I(x,y) in units of $\mu J/cm^2$. In general, the photocathode of a vidicon tube is not necessarily equally sensitive at all points, i.e. equal grey levels may not correspond to areas of equal brightness in the original image[16].

The first item that had to be examined was the system noise. By illuminating different portions of the screen with light and examining the pixel values of the resultant pictures, it was found that the noise was strictly additive i.e. $g = f + v$, where the input picture f and the noise v are uncorrelated. The noise itself was composed of two

parts: the first, a uniform background level that was essentially constant over the full picture and hence could be subtracted out; the second, a random pattern of shot noise which made the value of each pixel on the screen vary by as much as 15 counts (out of 256) from its neighbours. This shot noise, however, can be reduced by averaging over a number of points. Averaging over n points should reduce the standard deviation of the noise by the factor $\sqrt{n}$.

The next step was to determine the transfer function response of the camera/scintillator assembly. To accomplish this task, the imaging system was placed in the configuration shown in Figure 4.1. The entire surface of the scintillator was irradiated with a uniform illumination of ultraviolet light which was formed by passing the KrF laser light through two diffuser plates, placed 132 cm from the scintillator. The diffusing characteristics of the plates were previously measured using small (5 mm^2) photodiodes at various angles from normal.

By changing filters F_1 and F_2 a number of different light intensities were generated and the energy associated with each shot was cross-calibrated with calorimeters C_1 and C_2. Beam splitters BS_1 and BS_2 reflected 90% and 98% of incident energy respectively. BS_2 was a quartz flat which reflected 4% of the incident energy off each surface, for a total of 8%. From these tests, the camera's response was found to be of the form $I(x,y) = T(z) \times F(x,y)$ where $z = P(x,y)$ is the digitized intensity value at the pixel

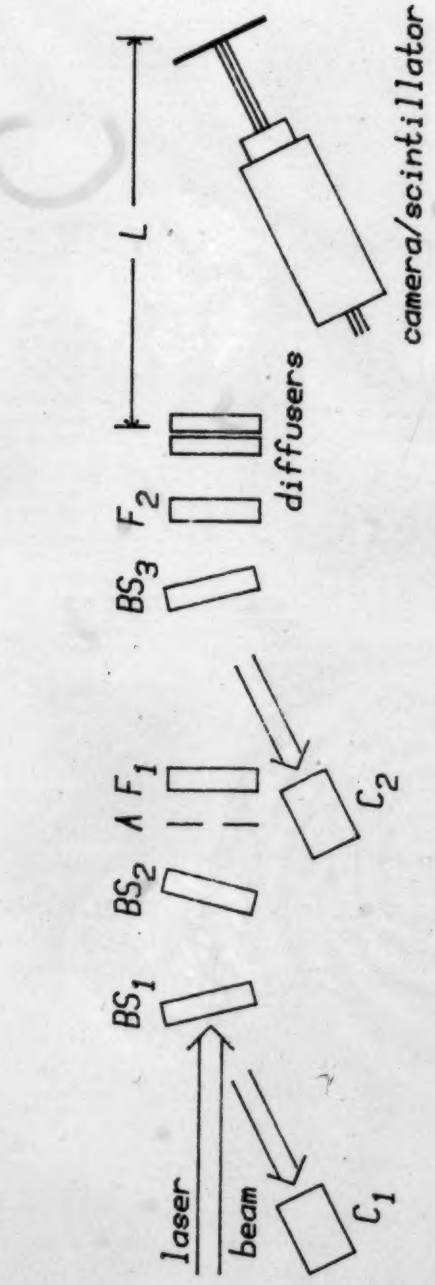


Figure 4.1 Calibration geometry.

x,y, T(z) is the transfer function of the vidicon camera to the intensity value z and F(x,y) is a correction factor which varies over the entire image.

To determine the transfer functon T(z), a number of different parts of the image were examined and the average value of each of these areas were calculated. After correcting for the different energy levels associated with each shot, a curve was drawn between the data points giving the transfer function in arbitrary units (see Figure 4.2).

The correction factor F(x,y) was much more difficult to characterize. Attempts to use a least-squares fit to equations such as $F(x,y) = 1/[k_1(x-x_0)^2+k_2(y-y_0)^2]$, failed to produce a good fit to the data. Finally, a two dimensional array of 17×17 elements was used for a simple numerical fit to an area of 224×224 pixels. The edges of the image were rejected for analysis purposes because of their large deviation from the mean response at the center of the field of view. Within this area, the camera response varied from a high of 147% (near the centre) to a low of 25% (lower left corner) of the average response. From these values, a bilinear interpolation was then performed to calculate the correction factor for an individual picture element. With this simple method a standard deviation of roughly 3% was achieved over the entire analysis area.

With the diffusers removed from the system, the laser beam was imaged directly on the fluorescent screen. The beam was then absolutely cross-calibrated with known photodiodes

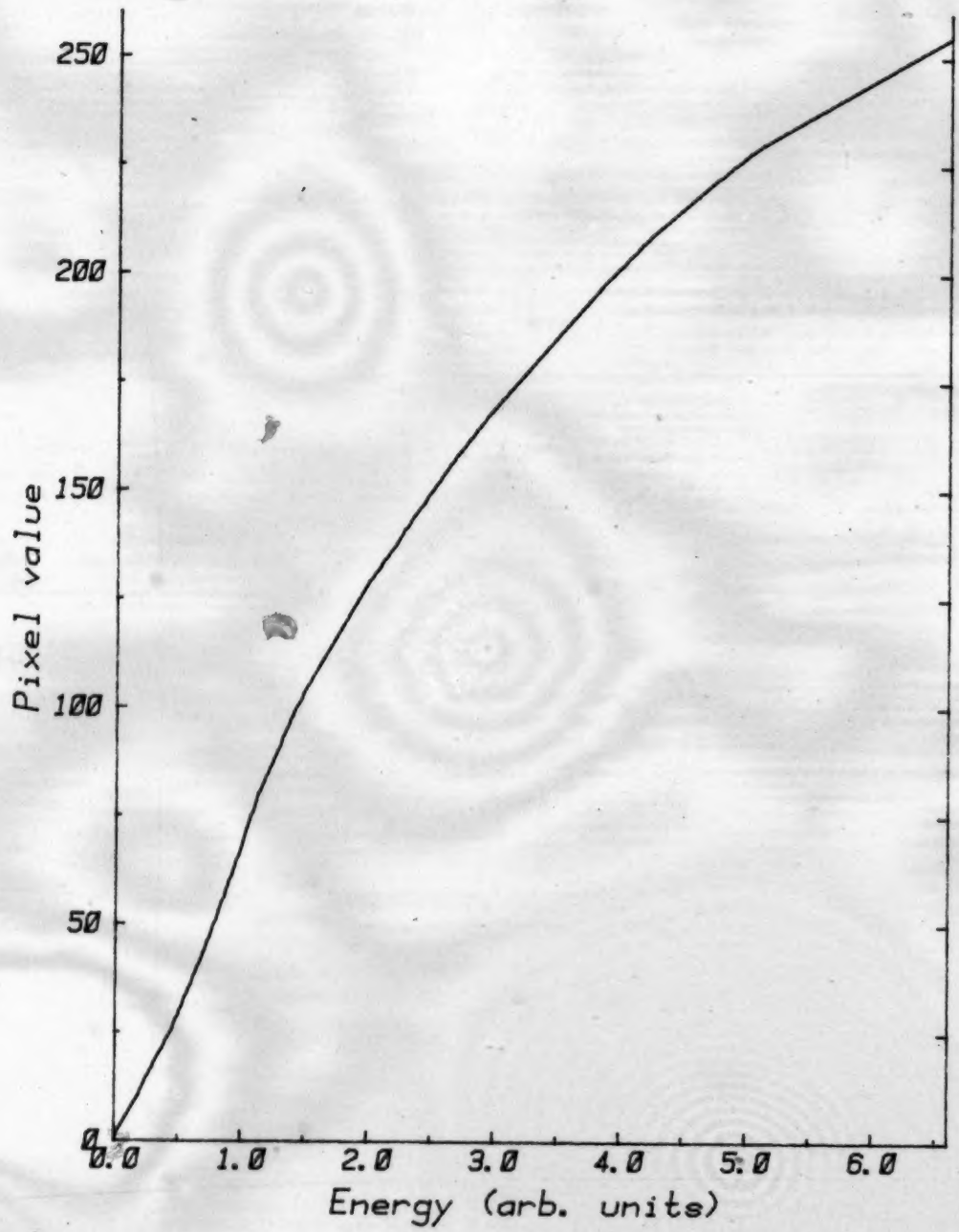


Figure 4.2 Transfer function of vidicon camera.

and calorimeters, using suitable neutral density filters of previously determined transmission coefficients. From these tests the transfer function T(z) could then be recomputed from arbitrary units into real integrated intensity values in units of μJ/pixel. The transfer function of the vidicon camera used for these experiments is shown in Figure 4.2 and has an accuracy of ±5% due to the calorimeters with which it was referenced to.

Finally, the beam was sent through a square aperture of width 17.9 mm in order to determine the geometrical scaling factors, both horizontally and vertically. By examining the digitized image and taking into consideration the angle of the plate w.r.t. the laser beam, these factors came out to be 3.9 pixels/mm (260 μm/pixel) in each direction, or 1521 pixels/cm². Horizontal and vertical slits of width 150 μm were introduced into the beam to discover the limiting resolution of the system, which turned out to be a single pixel wide.

4.2 Spatial measurements

All spatial and spectral measurements are carried out automatically by the program *ANALYZE* when requested from command mode. Both the spatial and spectral analysis routines divide the screen into 32 *anrows*. Each anrow (ANalyzed ROW) consists of 7 individual rows averaged together for noise reduction and contains 224 elements. For

example, the pth element of anrow #15 is given by

$$A_{15}(p) = 1/7 \sum_{i=0}^{i=6} P(p, 15\times7+i), \qquad (4.1)$$

where P(x,y) is the digitized pixel value at the point x,y. For further information regarding these routines, consult Appendix 2.

While undergoing spatial analysis, each element of each of the 32 anrows are processed and then categorized as to the energy density range that it falls into, and the # of occurrences in each range are stored in memory and used to histogram the % of total energy vs. energy density levels ($\mu J/cm^2$). These values are also used to determine the mean energy density and the standard deviation from that value.

Each of the 32 anrows are also subdivided into 32 subsections, to produce a 32 x 32 array of elements each of which consists of the average energy density over an area of 7 x 7 pixels. This 2D array, which can be optionally dumped to the line printer to be used as a low resolution map of the image, is scanned for maximum and minimum energy density levels and the entire array is totalled in order to calculate the total amount of energy that has fallen on the screen.

Finally, the raw image on the screen is replaced by a 3D representation of the processed image, complete with hidden line removal. Alternate anrows are displayed, with a z-shift of 1 pixel for every 0.1 $\mu J/cm^2$. This is an invaluable aid in identifying detailed features of the laser

profile, i.e. locating hot spots in the beam.

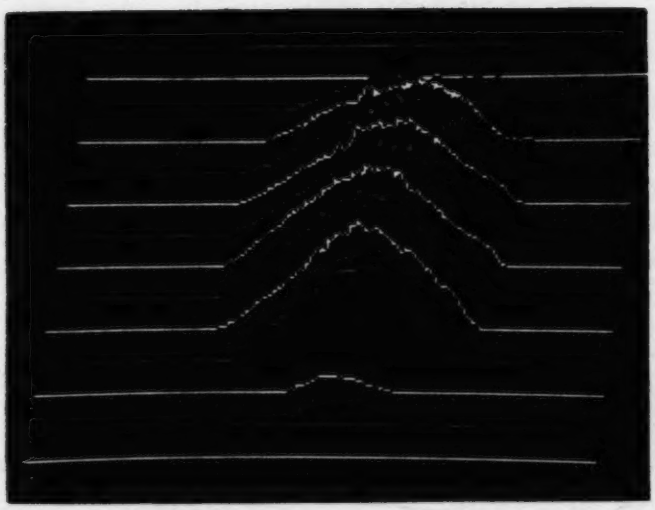
A complicating factor, however, is the effect of background room light. This background light, which is kept to a minimum by shielding the scintillator plate from direct room light, adds to the uniform noise level of the system. An additional problem is that the noise level is not constant, but gradually rises as the temperature of the vidicon tube in the camera rises. To compensate for this variation in the background noise level, the noise level must be periodically checked and the system noise variable adjusted to reflect the new value. During the course of these experiments, the system noise varied from a minimum of 2 counts to a maximum of about 35 counts (out of a maximum of 256 counts available).

To examine the spatial profile of the KrF laser beam, the camera/scintillator assembly was placed in the same position as shown in Figure 4.1, except with the double diffusers removed from the beam path. The scintillator screen was placed so as to make an angle of 25° between the normal and the beam path. Appropriate filters were placed in the beam in order to keep the light intensity below the camera's saturation level.

For the laser shot shown in Figure 4.3, the system noise level was determined to be 30±1 counts. With this level, the peak integrated intensity was found to be 4.76 ± 0.24 $\mu J/cm^2$, the mean was 2.82 ± 0.14 $\mu J/cm^2$ with a standard deviation of 1.14 ± 0.06 $\mu J/cm^2$. The total energy



(a)



(b)

Figure 4.3 Spatial profile of the KrF laser beam (a) before processing, and (b) after processing.

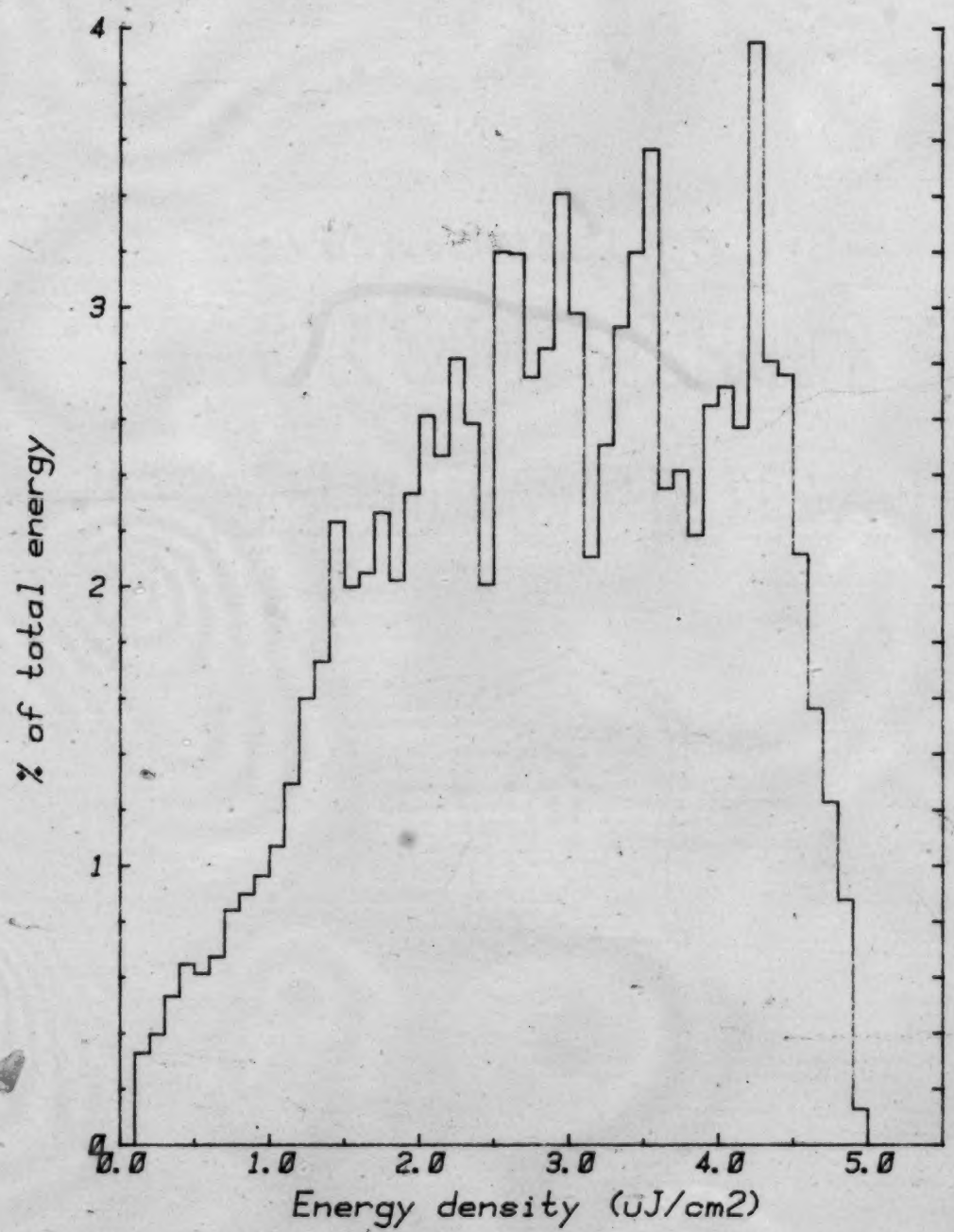


Figure 4.4 Energy density histogram of the sampled KrF laser beam.

that had been dumped on the scintillator screen was 18.06 ± 0.90 μJ. After considering all system losses due to mirrors, filters and quartz flats that lie along the beam path, this translates to a main beam energy of about 360 ± 18 mJ.

As can be seen in Figure 4.3, the intensity varied considerably over the entire laser beam. The histogram, shown in Figure 4.4, reflects this nonuniformity in the beam. The hole near the centre of the beam is due to the unstable resonator M_2 (see Figure 3.1). There were also a number of hot spots present in the beam, which were due in part to a gradual buildup of material on the inside of the injection-locked amplifier's CaF_2 windows. Although the total energy in the laser beam changed from shot to shot, the overall profile of the laser beam stayed relatively constant. No improvement in the uniformity of the laser beam was found until the lasers underwent a routine overhaul and the amplifier's windows were cleaned.

4.3 Spectral measurements

For all of the spectral measurements reported here, the Fabry-Perot interferometer was used in the configuration shown in Figure 2.4(b). Instead of a single lens to provide divergence of the beam, however, a pair of lenses were used: a negative lens with a focal length of -10 cm, and a positive lens with a focal length of +25 cm. By altering the

spacing between the two lens, the effective focal length f of the compound lens could then be easily altered. This provided a means not only of controlling the screen-source distance L but the light intensity as well, since the intensity drops off as $(L/f)^2$.

The routine for spectral analysis processes a pre-determined anrow whose fringes should be perpendicular to that anrow (i.e. the anrow is centred vertically on the Fabry-Perot fringe pattern). Since each anrow is actually the average of 7 consecutive rows of image data, the further off-centre the anrow is w.r.t. fringe centre the wider the fringes will appear after averaging.

All maxima in the row are identified as such and their positions are stored in memory. The criterion for determining maxima is that the magnitude of each maxima and minima must be separated by the factor *threshold*. From these maxima, a least-squares fit is used to find the order of the fringes from equation (2.14) which relates the fringe order to the fringe diameter. Once the order of each fringe is known, its instrumental linewidth can be calculated from Figure 2.5.

Since for $t/L \geq 10^{-4}$ the instrumental linewidth increases rapidly as the order increases, the program calculates the laser linewidth on the basis of the first complete fringe closest to the centre of the fringe pattern. As the routine currently requires the fringe centre to be located off to the right of the picture for proper order

identification, the fringe closest to the centre is then the rightmost fringe in the scanned area.

The observed linewidth $\Delta\nu_1$ in orders is found by locating the two half-intensity points of the fringe being analyzed, converting their positions into orders and then calculating $\Delta\nu_1 = n_1 - n_2$. The actual laser linewidth $\Delta\nu$ is subsequently calculated using the *Gaussian approximation* $\Delta\nu^2 = \Delta\nu_1^2 - \Delta\nu_2^2$, where $\Delta\nu_1$ is the observed linewidth and $\Delta\nu_2$ the instrumental linewidth. This approximation is valid for the deconvolution of Gaussian linewidths when $\Delta\nu_1 >> \Delta\nu_2$.

The accuracy with which the linewidth may be determined is also limited by the resolution of the system. The best one can hope for is to identify the raw linewidth to $n \pm 1/2$ pixels. Thus an accuracy of $1/2n$ can be expected.

Another important parameter is the % of the laser beam's energy that has been successfully injection-locked. As was shown in Chapter 2.2, only those portions of the KrF laser beam that have a narrow linewidth, i.e. have been injection-locked, will be efficiently compressed via backward Raman compression techniques. The % injection is computed by the following formula:

$$\% \text{ INJ} = \frac{\Delta\nu(1-min)}{min + \Delta\nu(1-min)} , \qquad (4.2)$$

where $\Delta\nu$ is the observed linewidth in orders and *min* is the average of the minima (each averaged over 3×7 pixels) located between the fringes normalized w.r.t. their respective maxima. This formula relies on the energy per

fringe in the injected signal being approximately described by $v(1-m/n)$ × fringe maxima. For greater accuracy the energy in the injected signal should be calculated by integrating the Fabry-Perot fringe pattern over one fringe order.

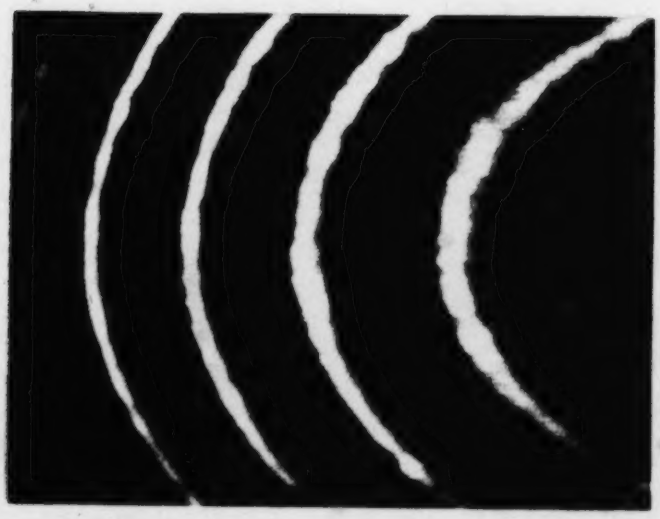
Measurements were taken of the resulting linewidth when the oscillator is controlled by only 2 etalons (see Figure 4.5(a)) and when controlled by all 3 etalons (see Figure 4.5(b)). Horizontal slices through the centre of the fringe pattern are shown in Figures 4.6 and 4.7 respectively. Note that the structure that is visible in the horizontal scans is also present in the raw data which is a real effect and not due to noise alone. It remains unclear at this time, however, how much of the structure is due to the spectral lineshape of the KrF laser and how much is due to the secondary fringes that arise because of the arrangement of the Fabry-Perot etalons (see Figure 2.5).

In the 2 etalon case, the plates of the Fabry-Perot interferometer were separated by a distance t = 6.0 mm, providing a free spectral range (F.S.R.) of 0.83 cm^{-1} or 25.0 GHz. The effective screen-source distance L was 4.0 m, hence $t/L = 1.5\times10^{-3}$. The fringe pattern shown in Figure 4.5(a) was found to be centred on *anrow* #13, which is graphed in Figure 4.6 after conversion to real intensity values.

From spectral analysis, the fringe centre was calculated to be at x = 218 and the order of the innermost fringe on the screen was N_o = 0.20. Consequenty, from Figure



(a)



(b)

Figure 4.5 The output of a Fabry-Perot interferometer of the KrF laser controlled by (a) 2 angle-tuned etalons E_1, E_2 and (b) 3 angle-tuned etalons E_1, E_2 and E_3.

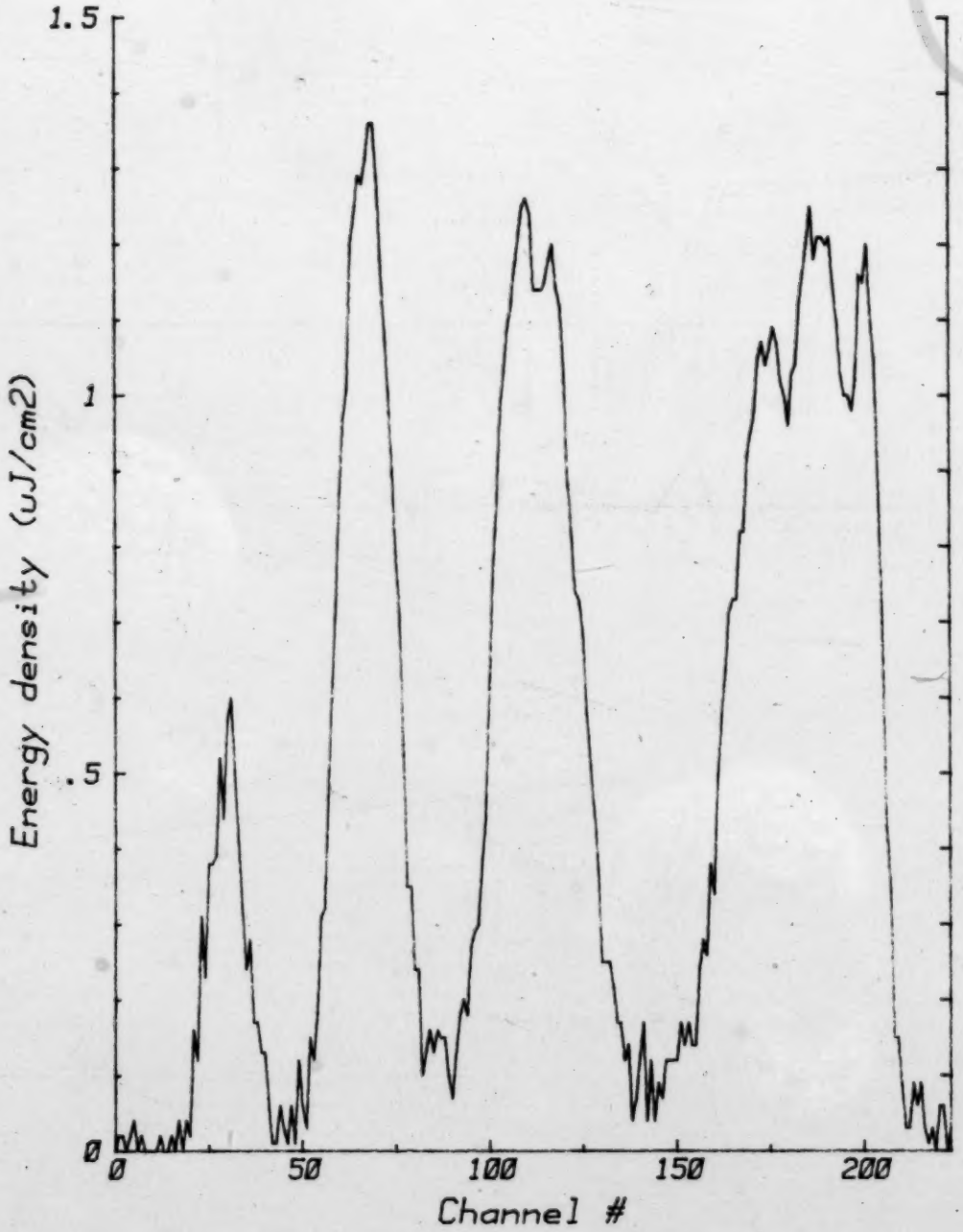


Figure 4.6 Horizontal scan through the centre of the fringe pattern of Figure 4.5(a).

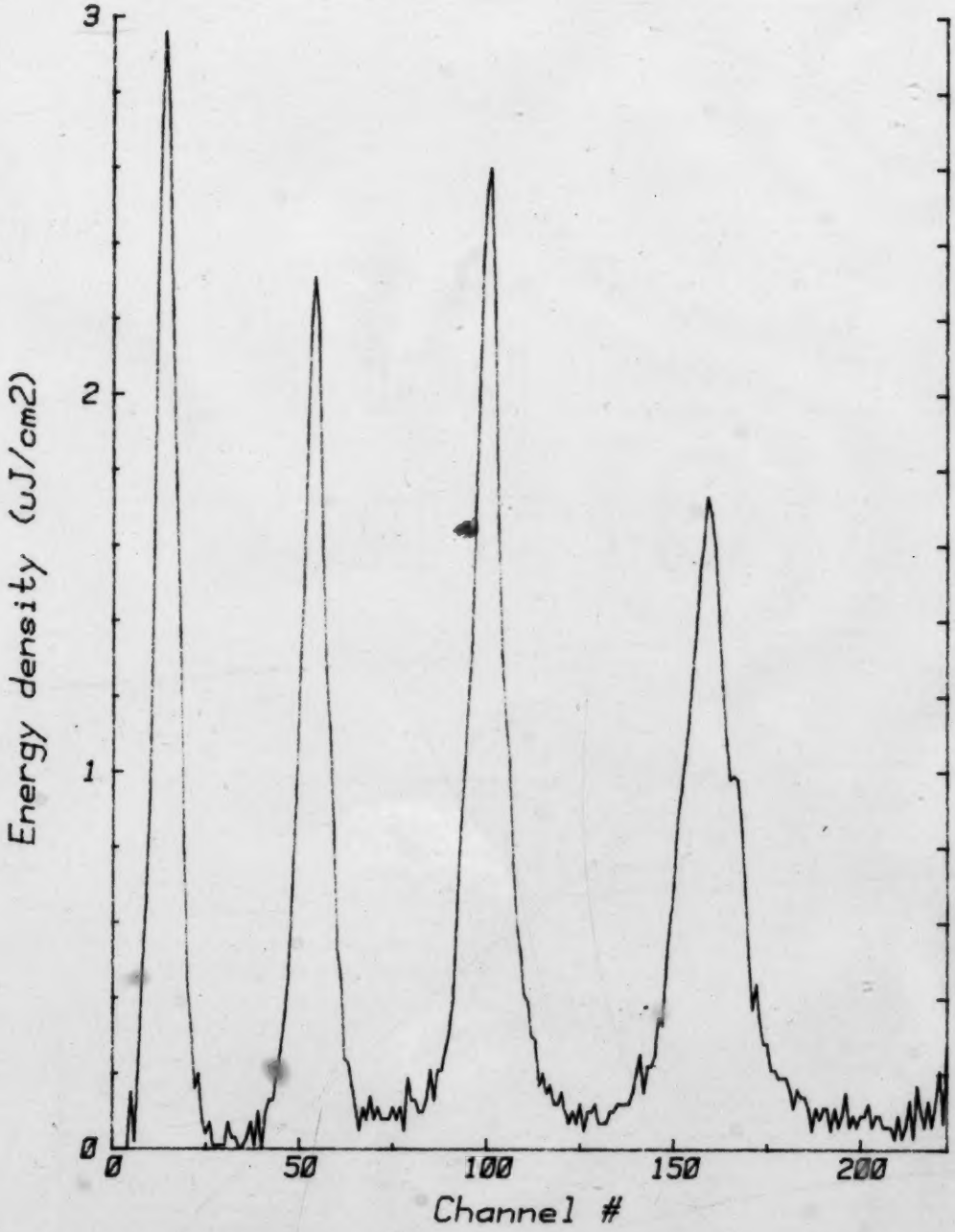


Figure 4.7 Horizontal scan through the centre of the fringe pattern of Figure 4.5(b).

2.6, the instrumental linewidth for our $p(t/L) = 0.3\times10^{-3}$ is 0.04 orders or 1.0 GHz. Thus the FWHM linewidth $\Delta\nu$ was determined to be 8.4 GHz or 0.28 cm^{-1}, with 92 ± 5% injection with a system noise level of 3 ± 1 counts.

In contrast, for the 3 etalon case, t was set to 1.50 cm, providing an F.S.R. of 0.33 cm^{-1} or 10.0 GHz. The screen-source distance L was 7.0 m, hence $t/L = 2.1\times10^{-3}$. The fringe pattern shown in Figure 4.5(b) was centred on *anrow* #15, which is graphed in Figure 4.7. The fringe centre was calculated to be at x = 330 and $N_o = 1.24$. For the corresponding $p(t/L) = 2.6\times10^{-3}$, the instrumental linewidth is 0.09 orders or 0.9 GHz. We therefore find a FWHM linewidth $\Delta\nu$ = 2.1 GHz or 0.070 cm^{-1}, with 90 ± 5% injection with a system noise level of 3 ± 1 counts.

With only two etalons controlling the oscillator, the laser linewidth remained fairly constant during these experiments with values in the range of 8-9 GHz (0.27 - 0.30 cm^{-1}) and injection levels of 85-95%. With three intracavity etalons, however, the system became more susceptible to timing jitter between the trigger signals of the oscillator and the amplifier modules. Linewidths ranged from 1.1 - 2.8 GHz (0.04 - 0.10 cm^{-1}) with injection levels that varied from 40-95%. It must be noted, however, that the lower values were obtained by subtracting large instrumental linewidths from the observed linewidths and the accuracy is therefore limited.

4.4 Discussion

For accurate measurements, the system noise level must be closely monitored, since this is a major source of error in both spatial and spectral analysis routines. The system noise of the camera has been found to rise at a rate of up to 4 counts per hour, depending on room temperature. For spectral measurements, however, an even greater source of potential error is caused by high values of $p(t/L)$ which broaden the instrumental width of the fringes. Care must be taken to keep t/L as small as possible, preferably much less than 10^{-3}.

An additional factor to be concerned about is the effect that the number of fringes in the analysis area has on the linewidth measurements. Although widely spaced fringes will tend to increase the accuracy with which the linewidths may be determined, a minimum of 3 fringes must be present in the scanned area for proper fringe identification. Furthermore, 4 fringes are needed to correctly determine the fringe orders to less than 5% of an order.

5. CONCLUSIONS AND RECOMMENDATIONS FOR FURTHER WORK

An optical imaging system has been designed to meet a variety of experimental requirements and subsequently used to determine the spatial and spectral characteristics of a krypton fluoride (KrF) discharge laser system. Narrow linewidth (0.07 cm^{-1}) outputs were measured in 20 ns FWHM laser pulses with energies of 360 mJ. The narrow linewidth operation of the laser was achieved by placing a stack of angle-tuned etalons inside the laser cavity of the master oscillator. Finely detailed spatial structure in the laser beam was resolved to areas of the order of 1 mm^2.

Hardware was implemented to allow a microcomputer to control the video digitizer system through its parallel port. A hand-toggle programming unit was designed and assembled to either allow the user to toggle in read/write instructions directly, or to act as a buffer unit between the host computer and the video digitizer system. Additional circuitry was developed to permit the interface unit to trigger the laser in conjunction with digitization of the video output of a monitoring camera.

All software was written for the system, including special routines written in both C and MC68000 machine language to manipulate the parallel port data and control lines. The final software package that was developed allows the user to analyze the spatial profile of the laser beam, or to examine the interference fringes that appear after passing the laser light through an ultraviolet Fabry-Perot

interferometer, thereby determining the laser linewidth.

These image analysis routines have in turn been combined with others which control and interpret CAMAC data acquisition modules present in an external CAMAC crate, into a single master control program which can trigger the laser, analyze the digitized images from the vidicon camera, monitor the timing of various components of the KrF laser chain and display energy readings obtained from a number of photodiodes and calorimeters.

One system composed of a visible light vidicon camera and a scintillator screen was completely calibrated for response to ultraviolet laser light. The system was tested and used for the experimental analysis of KrF laser profile and spectra.

A major improvement to the system would be to use cameras which are sensitive to direct exposure with ultraviolet light. At the time of writing, the laboratory is in the process of modifying two fibre-optically coupled cameras from RCA so that they will respond directly to ultraviolet light. When this has been accomplished, the cameras can be calibrated in a similar fashion to that used for this work. Furthermore, the Fabry-Perot configuration should be altered to that of Figure 2.4(a) since this will decrease the instrumental linewidth to a smaller value (0.034 orders). The small size of the fringe pattern ($\leq$4 cm) and the significantly lower light levels that this configuration will produce pose no difficulty, since the

sensing area of the vidicon is only about 1.5 cm in diameter and will respond to quite low levels of direct illumination.

Another improvement that could be made is in the deconvolution of the spectral linewidth. Although the Gaussian approximation is quite useful and simple to use, it does not work reliably with non-Gaussian profiles. A pseudo-deconvolution such as that performed by Jones et. al.[17] should not prove too difficult to implement.

For faster processing of pictures, a high speed Multibus extender could be used to couple the MATROX and CAMAC cards into the main system bus. By not having to pass all instructions through the parallel port, data transfer times could probably be halved (at the very least).

Finally, there is the problem of limited resolution. Although the current 256 × 256 resolution is quite adequate for spatial analysis, higher resolution would greatly increase the accuracy of the spectral analysis routines. Should the decision be made to upgrade the system, there are a number of manufacturers that now produce a 512 × 512 resolution video digitizer system, including MATROX. Such a system would essentially double the accuracy of all measurements made with the current system. In addition, the two systems could be used at the same time for simultaneous spatial and spectral analysis.

REFERENCES

[1] C. Garban-Labaune, E. Fabre and A. Michard, "Effect of target material on absorption measurements at short laser wavelengths," *Opt. Commun.*, vol. 41, pp. 174-177, 1 April 1982.

[2] Francis F. Chen, *Introduction to Plasma Physics*, pp. 279-318, Plenum Press, New York 1974.

[3] D.R. Speck, E.S. Bliss, J.A. Glaze, J.W. Herris, F.W. Holloway, J.T. Hunt, B.C. Johnson, D.J. Kuizenga, R.G. Ozarski, H.G. Patton, P.R. Rupert, G.J. Suski, C.D. Swift, and C.E. Thompson, "The Shiva laser-fusion facility," *IEEE J. Quantum Electron.*, vol. QE-17, pp. 1599-1619, September 1981.

[4] J.P. Carpenter, D.E. Casperson, R.B. Gibson, R.P. Godwin, R.F. Haglund, Jr., J.A. Hanlon, E.L. Jolly, and T.F. Stratton, "Helios: a 15 TW carbon dioxide laser-fusion facility," *IEEE J. Quantum Electron.*, vol. QE-17, pp. 1662-1678, September 1981.

[5] R.L. McCrory, "Implications of Short Wavelength Laser Matter Interaction Experiments on Ignition," *Bull. of Am. Phys. Soc.*, vol. 26, p. 972, 1981.

[6] M. Rokni, J.A. Mangano, J.H. Jacobs, and J.K. Hsia, "Rare gas fluoride lasers," *IEEE J. Quantum Electron.*, vol. QE-14, pp. 464-481, 1978.

[7] J.J. Ewing, R.A. Haas, J.C. Swingle, E.V. George and W.F. Krupke, "Optical pulse compressor systems for laser fusion," *IEEE J. Quantum Electron.*, vol. QE-15, pp. 368-379, May 1979.

[8] J.R. Murray, J. Goldhar, D. Eimerl and A. Szoke, "Raman pulse compression of excimer lasers for application to laser fusion," *IEEE J. Quantum Electron.*, vol. QE-15, pp. 342-368, May 1979.

[9] D.C.D. McKen, R. Fedosejevs, M. Arnfield, I.V. Tomov, C. Domier, and A.A. Offenberger, "An electrically triggered multi-module KrF laser system with narrow linewidth output," (to be published).

[10] I.V. Tomov, R. Fedosejevs, D.C.D. McKen, C. Domier, and A.A. Offenberger, "Phase conjugation and pulse compression of KrF laser radiation by stimulated Raman scattering," *Opt. Lett.*, vol. 8, pp. 9-11, January 1983.

[11] J.R. Murray, J. Goldhar, and A. Szoke, "Backward Raman gain measurements for KrF laser radiation scattered by CH_4," *Appl. Phys. Lett.*, vol. 32, pp. 551-553, 1978.

[12] Max Born and Emil Wolf, *Principles of Optics*, pp. 323-329, Pergamon Press, Toronto, Fourth edition 1970.

[13] S. Tolansky, *Multiple-Beam Interferometry of Surfaces and Films*, pp. 171-177, Oxford University Press, London, 1948.

[14] R. Fedosejevs, I.V. Tomov, D.C.D. McKen, M. Arnfield, C. Domier, A.A. Offenberger, "Narrow-linewidth gain and saturation measurements of a KrF discharge laser", (to be published).

[15] James A.R. Samson, *Techniques of VACUUM ULTRAVIOLET SPECTROSCOPY*, pp. 212-216, John Wiley & Sons, Inc., New York 1967.

[16] Azriel Rosenfeld, Avinash C. Kak, *Digital Image Processing*, pp. 162-197, Academic Press, 1976.

[17] R.N. Jones, R. Venkataraghavan and J.W. Hopkins, "The control of errors in infrared spectrophotometry - I. The reduction of finite spectral slit distortion by the method of 'pseudo-deconvolution'", *Spectrochimica Acta*, vol. 23A, pp. 925-939, Pergammon Press 1967.

APPENDIX 1. HAND-TOGGLE PROGRAMMING UNIT

The hand-toggle programming unit was designed to be used in conjunction with the external interface of the FG-01 video digitizer board from MATROX in either of two modes: as a stand-alone unit to hand-toggle read/write instructions directly; or as a buffer unit to relay instructions from the main computer. At the back of the unit are two 25 pin D-style connectors: connector P1 is designed to be joined to a similar connector at the back of the Multibus cardcage while connector P2 is to be joined to the parallel port of the main computer.

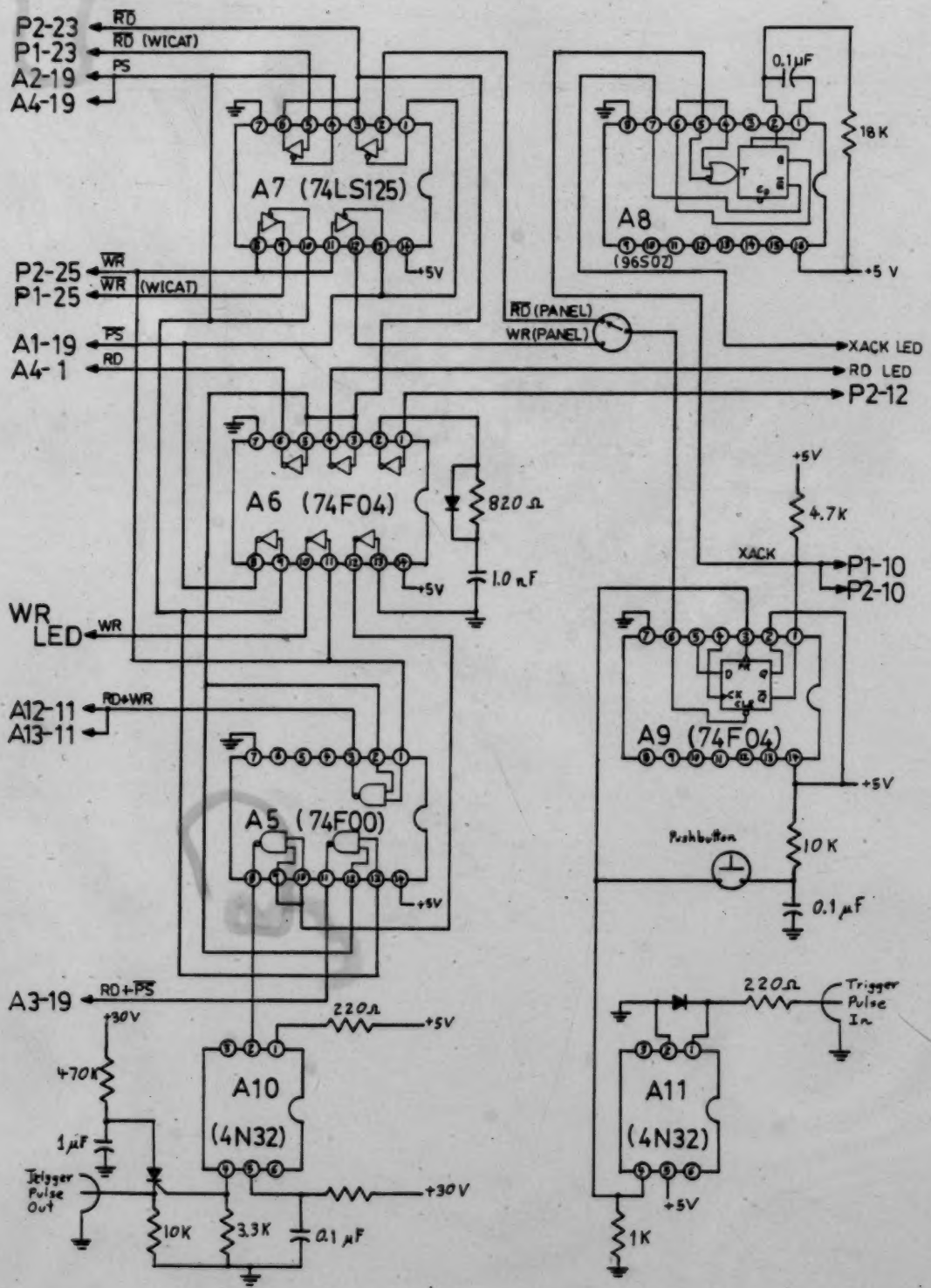
The two connectors were originally designed to be pin-compatible with the parallel port on the WICAT, but this resulted in cross-talk between the various control lines (RD, WR, XACK). This was solved by rewiring the connector to interpose ground lines between all of the control lines. This was easily done to the Multibus connector, while a small box was made and placed over the Wicat parallel port connector to cross-connect these lines back again.

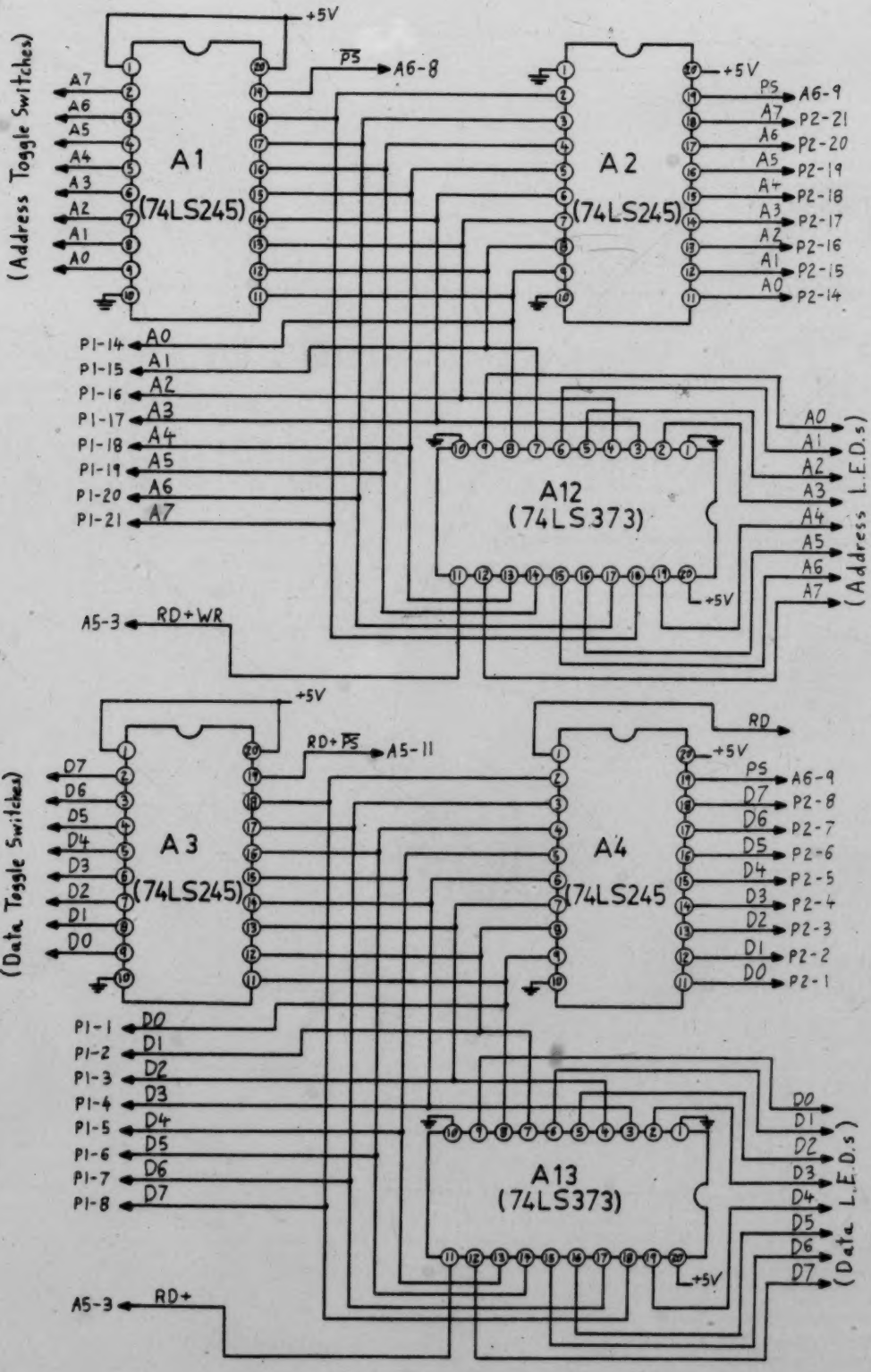
On the front panel are three sets of switches, three sets of LEDs (light emitting diodes), a momentary switch and a power switch. The first set of switches lets the user set the 'manual/Wicat' mode, 'read/write' mode and 'trigger/no trigger' mode. The second set controls the 8 address lines, and the third set controls the 8 data lines. The first set of LEDs is composed of 3 LEDS which light up in response to

signals on the RD, WR and XACK control lines. The second set of LEDS show the address of the last operation, and the third set shows the data that was either written or read back.

To control the system manually, the 'manual/Wicat' switch is set to the manual position. The 'read/write' toggle switch controls the type of operation which is triggered either by the momentary switch or by a pulse coming in from a BNC connector on the back of the unit. For a read operation only the address switches have to be set, while for a write operation both the address and data switches have to be set.

To allow the system to trigger the laser-firing sequence, one of the lines on the P1 connector is connected up to a signal on the FG-01 board which goes low upon the start of an erase or digitize command. The 'trigger/no trigger' switch switches in/out a 30 Volt battery which supplies the power for the trigger pulse. The trigger pulse comes out another BNC connector on the back of the unit.


P2-23
P1-23
A2-19
A4-19
RD
RD (WICAT)
PS
A7 (74LS125)
+5V
P2-25
P1-25
WR
WR (WICAT)
A1-19
A4-1
PS
RD
A6 (74F04)
820 Ω
1.0 nF
+5V
WR LED
WR
A12-11
A13-11
RD+WR
A5 (74F00)
+5V
A3-19
RD+PS
+30V
470K
1 μF
Trigger Pulse Out
220 Ω
+5V
A10
(4N32)
10K
3.3K
0.1 μF
+30V
0.1μF
18K
A8
(96S02)
+5 V
RD (PANEL)
WR (PANEL)
XACK LED
RD LED
P2-12
+5V
4.7K
XACK
P1-10
P2-10
A9 (74F04)
+5V
Pushbutton
10 K
0.1 μF
220 Ω
Trigger Pulse In
A11
(4N32)
+5V
1K


(Address Toggle Switches)
A1
(74LS245)
A2
(74LS245)
+5V
P5
A6-8
A7
A6
A5
A4
A3
A2
A1
A0
PS
A6-9
P2-21
P2-20
P2-19
P2-18
P2-17
P2-16
P2-15
P2-14
P1-14
P1-15
P1-16
P1-17
P1-18
P1-19
P1-20
P1-21
A12
(74LS373)
(Address L.E.D.s)
A5-3
RD+WR
(Data Toggle Switches)
A3
(74LS245)
A4
(74LS245
RD+P5
A5-11
RD
D7
D6
D5
D4
D3
D2
D1
D0
P2-8
P2-7
P2-6
P2-5
P2-4
P2-3
P2-2
P2-1
P1-1
P1-2
P1-3
P1-4
P1-5
P1-6
P1-7
P1-8
A13
(74LS373)
(Data L.E.D.s)
RD+

```
*****************************************
*          ANALYZE USERS MANUAL         *
*               Version 1.0             *
*             Calvin W. Domier          *
*     Dept. of Electrical Engineering   *
*          University of Alberta        *
*                March  1983            *
*****************************************
```


1. OVERVIEW.....67

2. COMMAND SUMMARY.....67

3. COMMAND DESCRIPTIONS.....68

   3.1 HELP command.....68

   3.2 FIRE command.....68

   3.3 TDC command.....68

   3.4 ADC command.....68

   3.5 GRAPH command.....68

   3.6 MATROX command.....69

   3.7 CALIBRATE command.....70

   3.8 XFER command.....71

   3.9 DUMP command.....71

   3.10 VIDEO PIXEL EDITOR command.....71

   3.11 PARMS command.....71

   3.12 EXIT command.....72

1. OVERVIEW

ANALYZE is a program designed to allow the user to fire the laser, digitize an image from a video camera and then perform a number of analysis functions on the image. The program also allows the user to analyze data gathered from a number of CAMAC modules, including Time-to-Digital Converters (TDC 2228A) and Analog-to Digital Converters (ADC 2232C).

The program is designed to be run in background mode, by the command

&/ANALYZE .

The source code is written in C and MC68000 assembler code, and is contained within the following source files:

ANALYZE.C	- contains the analysis and control routines;
CAMAC.C	- contains the subroutines to access CAMAC data aquisition modules;
PORT.C	- contains low order imaging routines such as r_pixel, w_pixel, etc.
DRIVER.S	- contains MC68000 assembler routines to allow the program to enter and exit supervisor mode.

The program is controlled from the device 'MONITOR', which is set to a CYBERNEX XL-87D terminal. Output may also be directed to the device 'PRINTER', which is expected to be an EPSON MX-80 dot-matrox printer with the GRAFTREX option. It is designed to run simultaneously with the program STATUS which keeps a continuous monitor on many of the voltages and currents in the laser modules.

2. COMMAND SUMMARY

All commands are entered by pressing a single keystroke. The commands currently implemented are:

h:	HELP command
^f:	FIRE command
t:	TDC command
a:	ADC command
1-0:	GRAPH command
m:	MATROX ANALYSIS command
c:	CALIBRATE command
x:	XFER command
d:	DUMP command
v:	VIDEO PIXEL EDITOR command
p:	PARMS command
e:	EXIT command

Any keypress that does not have a corresponding command will default to the HELP command.

3. COMMAND DESCRIPTIONS

3.1 HELP command

This command displays the list of commands available in the current implementation. A brief description of each is also given.

3.2 FIRE command

The fire command fires the laser, digitizes a preset number of video frames from the vidicon camera and gathers data from both the TDC 2228A time-to-digital converters and the ADC 2232C time-to-digital converters on the CAMAC crate. The frame# (# of video frames that are digitized) can be altered with the 'p1' command (see 3.11.1). Only the final digitized frame will remain stored in video memory. NOTE: a frame# = 0 will result in no frames being digitized and will thus NOT fire the laser!

Immediately following these steps, the routine continues automatically with the TDC command (see 3.3).

3.3 TDC command

This command displays the timing results gathered from the previous laser shot and computes the energy readings from 8 calorimeters in the laboratory that occupy ADC channels 1-8. The CAMAC slot# of the TDC unit to be analyzed is preset by the 'p3' command (see 3.11.3).

3.4 ADC command

This command displays the ADC channel data from the previous laser shot. The data is paged through 14 cycles at a time, with up to 8 channels being displayed simultaneously. Associated with each cycle is a number which represents the time in milleseconds relative to the firing of the laser. Cycles 0-2, which will show negative times, are read before the laser is fired and are used for baseline correction in calculating the calorimeter energy measurements (see 3.3 TDC command).

The number of cycles (ncycles) and the number of channels (nchans) read per cycle are preset by the 'p3' command (see 3.11.3). In no case should ncycles x (nchans + 1) > 650, as only 650 elements have been reserved for the ADC data.

NOTE: To reduce the effect of 60 Hz electrical noise, nchans should be adjusted so that the time between successive reads is about 8.33 msec. Averaging over two consecutive readins will effectively kill the noise.

3.5 GRAPH command

This command graphs the data gathered by the ADC scan. Pressing the keys 1-0 will graph ADC channels 1-10. The graph appears on the 'MONITOR' and its size is 34 x ncycles.

3.6 MATROX ANALYSIS command

This command lets the user perform one of 3 different MATROX analysis functions:

(1) - Spatial analysis
(2) - Spectral analysis
(3) - Single row scan.

All 3 MATROX routines divide the screen into 32 horizontal anrows (ANalyzed ROW), where each anrow is composed of 7 individual rows of 224 elements averaged together. The camera background level (see 3.11.1) is subtracting from each element, and the anrow is then analyzed in either processed mode (converted into real intensity values in uJ/cm2) or raw mode (analyzed in raw pixel counts / 100, i.e. 0.00-2.55).

3.6.1 Spatial analysis

The spatial analysis routine catagorizes each element of each of the 32 anrows as to the energy density range that it falls into, with the # of occurances in each range used to histogram the % of total energy vs. energy density levels. The histogram is displayed on the device 'MONITOR' and the values are used to determine the mean energy density and the standard deviation from that value.

If auto-fringe = 1 (see 3.11.2), then the image is also scanned to determine the vertical centre of the fringe pattern. This anrow value is then used for all future spectral scans.

The spatial analysis routine subdivides each of the 32 anrows into 32 subsections, to produce a low resolution 32 x 32 mapping of the image. This 2D array, which can be dumped to the 'PRINTER' (see 3.11.2), is scanned for maximum and minimum energy density levels and the entire array is totalled to calculate the total amount of energy in the image.

Finally, the original image is replaced by a 3-D representation of the image, complete with hidden line removal. Alternate anrows are displayed, with a z-shift of 1 pixel : 0.1 uJ/cm2 for processed data or 1 pixel : 10 counts for raw data.

3.6.2 Spectral analysis

The spectral analysis routine first locates all the fringe maxima in in the pre-selected anrow. Using a running average of 'neighbourhood' pixels, each maxima and minima must be separated by the factor 'threshold' (see 3.11.2). The threshold value should be kept high enough that noise effects do not introduce secondary fringes.

The position of the maxima are used to determine their respective fringe orders. This is done by a least-squares method and requires a minimum of 3 fringe maxima, although for best results 4 fringes should be used. After the location of fringe centre and the order #'s have been calculated, the user is prompted for approval. If the numbers do not seem reasonable, the user may enter in his own value for the location of fringe centre and the program will do a least-squares fit about this new value. This second least-squares fit may be taken with as few as 2 fringes and still provide a reasonable accuracy.

The row is then normalized so that all maxima are set to 1000. The minima and the half-maxima points (= [1000+min] / 2) are found between the maxima and the locations of the half-points N1 & N2 of each fringe are converted into orders, making the raw linewidth W1 = N1 - N2 in orders. Using the average values of min and W1 the % injection values are found by:

$$\% \text{ INJ} = \frac{W1 \times (1000 - \text{min})}{\text{min} + W1 \times (1000 - \text{min})} \times 100\%$$

The raw linewidth W1 is calculated for the innermost (rightmost) fringe, while the instrumental linewidth W2 is set by the value of NO(t/L) where NO is the order of the fringe and t/L is the ratio of the etalons spacing to the effective screen-source distance. The corrected linewidth WO is found using the 'Gaussian approximation' WO*WO = W1*W1 - W2*W2.

The maximum and minimum values, the # of maxima and the order NO of the innermost fringe being analyzed are displayed. Also displayed are the % injection, the free spectral range (F.S.R.) and the raw and corrected linewidths in GHz and a graph of the first 130 normalized elements.

3.6.3 Single row scan

Single row scan scans the row 'Anrow', computes the Max, Min and Avg values in that row and displays the selected row on the 'MONITOR'. The row is displayed in double density graphics 34 x 112, with each dot representing the average of 2 elements of the anrow.

3.7 CALIBRATE command

Assuming that the current image represents the camera's response to uniform illumination, this recalibrates the geometrical correction factor RESPONSE (x,y). It assumes that the camera responds as I (x,y) = INTENSITY [P (x,y) - noise] * RESPONSE (x/7,y/7) where INTENSITY [] is the transfer function response of the camera, P (x,y) is the pixel value at x,y and noise is the camera background level (see 3.11.1).

The new values are displayed on the 'MONITOR' and optionally on the 'PRINTER' and may replace the original values of RESPONSE. Each value represents the % response of that portion of the image compared to the average response of the entire image. The default values are:

58	67	75	82	87	92	97	106	112	116	116	117	116	112	108	102	94
62	73	83	88	93	98	105	113	118	123	125	124	122	118	113	107	98
64	76	88	95	99	103	110	120	127	130	132	133	129	124	116	110	104
66	79	90	100	104	108	115	124	133	139	139	138	136	127	121	114	106
69	83	94	103	110	114	120	130	136	142	146	147	141	133	124	118	108
68	84	96	106	113	116	124	133	141	146	147	146	144	136	125	119	109
68	82	95	106	115	121	129	136	142	145	146	147	143	136	125	115	106
67	80	94	106	115	125	133	140	145	145	143	143	139	132	120	109	103
66	78	90	102	114	123	131	137	139	140	138	137	133	127	114	106	98
62	74	85	96	106	116	123	127	131	132	134	132	128	122	113	102	92
58	70	80	89	98	108	111	117	122	124	126	125	121	114	108	97	88
54	65	75	83	91	100	104	108	112	117	120	117	112	107	102	91	82
49	59	70	79	87	94	98	101	108	111	109	107	103	99	93	84	74
44	55	66	75	81	88	93	99	102	103	102	99	95	92	85	75	66
39	50	59	66	73	79	85	89	94	95	94	92	89	85	77	69	62
33	44	52	58	65	71	77	82	85	85	86	85	81	76	70	63	58
25	36	44	51	58	65	70	73	75	79	77	74	70	67	63	58	50

3.8 XFER command

This command allows the user to transfer pictures to/from the WICAT. The user is first prompted for the direction of transfer, followed by the filename. The file is placed or searched for in a predetermined WICAT root directory which can be modified by the 'p4' command (see 3.11.4). Pictures take up 64K of disk memory to store a 256 x 256 x 8 bit image.

3.9 DUMP command

This command takes the picture stored in the MATROX video boards and dumps it to the device 'PRINTER', which is assumed to be an EPSON MX-80 printer with GRAFTREX. The picture can be reproduced with pseudo grey scales of 3, 5 or 9 grey shades. The height of the picture can be controlled, as well as the method of choosing the threshold values, by the command 'p5' (see 3.11.5).

3.10 VIDEO PIXEL EDITOR command

This command lets the user examine and alter the pictures on the MATROX video boards on a pixel by pixel basis. The monitor displays a window of 11 x 18 pixels, and a flashing cursor indicates the position of the window centre. The window may be moved in 8 directions by use of the numerical keypad whose range is set by the 'r' (RANGE) command. Alternatively, the window can be moved to an absolute position x,y with the 'm' (MOVE) command. The centre pixel in the window may be altered with the 'w' (WRITE) command.

A brief help file may be obtained by pressing the 'h' key. To leave the video pixel editor press the <ESC> key. NOTE: a left square bracket '[' will appear in the lower left corner of the display to indicate that the editor is in effect.

3.11 PARM command

This command lets the user change a number of system parameters. They are broken down into 6 basic types:

1 - camera	4 - rootdir
2 - matrox	5 - screen dump
3 - camac	6 - shot#

For all options (except #4 - rootdir), the return key may be pressed to skip that parameter without altering its value.

3.11.1 camera parameters:

Video camera # (0-3)	default value = 0
Camera background level (0-255)	default value = 3
Geometrical calibration factor # of pixels / cm2	default value = 1521
Energy calibration factor (all processed data is scaled by this factor)	default value = 34800
Video frame # to grab when firing laser (see 3.2 FIRE command)	default value = 1

3.11.2 matrox parameters:

Auto-printout (should a printout be generated automatically) (0=no, 1=yes)	default value = 0
Processed data (should the data be processed into units of uJ/cm2) (0=no, 1=yes)	default value = 1
Noise threshold level (= smallest difference allowed between minima and maxima)	default value = 35
Neighbourhood size (for determing fringe (for spectral analysis)	default value = 3
Spectral scan row# (0-31) (row# to be analyzed)	default value = 15
Auto-fringe (should spatial analysis search the image while processing to determine the spectral anrow) (0=no, 1=yes)	default value = 0
Screen-source distance (mm)	default value = 4000
Spacing of Fabry Perot (um)	default value = 6000

3.11.3 CAMAC parameters:

# of ADC channels to be scanned (1-16)	default value = 11
# of ADC cycles to be scanned (0-65)	default value = 55
TDC slot# in CAMAC crate (1-23)	default value = 1

3.11.4 rootdir:

This option lets the user set the default directory for picture transfers to/from the WICAT (see 3.8 XFER command). The directory name can be a maximum of 30 characters long. Most commonly used names are:

""	to transfer to the user's directory,
"_dx0/rootdir/"	to transfer to the floppy disk.

3.11.5 screen dump parameters:

This option allows the user to modify the parameters used to produce screen dumps of the video image to the printer (see 3.9 DUMP command).

# of grey shades (3,5,9)	default value = 3
Upper picture line# (0-255)	default value = 8
Lower picture line# (0-255)	default value = 239
Method of choosing threshold values: 1. Even spacing of values, 2. User specified values, 3. Computer selected values.	default value = 3

3.11.6 shot parameter:

This option allows the user to set the last shot#. This number gets incremented every time the laser is fired (see 3.2 FIRE command).

3.12 EXIT command

This command allows the user exit from the ANALYZE program.